Nonlinear Dyn (2022) 107:1545–1568
https://doi.org/10.1007/s11071-021-06381-8

ORIGINAL PAPER

Planar nonlinear dynamic analysis of cable-stayed bridge considering support stiffness

Houjun Kang · Xiaoyang Su · Zihao Pi

Received: 21 October 2020 / Accepted: 16 March 2021 / Published online: 27 March 2021

Abstract Support stiffness is one of important factors on structure dynamics. Considering the vertical support stiffness, a multi-cable-stayed shallow-arch model of the cable-stayed bridge is established. Its differential equation governing the planar motion of cables and the shallow arch and the boundary conditions are derived by Hamilton's principle. Firstly, the in-plane free vibration of the system is explored in order to find the modal functions and the possible internal resonances of nonlinear dynamics. Then, the 1:2:2 internal resonance among the different modes of the shallow arch and two cables are investigated by the multiple time scale method and pseudo-arclength algorithm. Meanwhile, the frequency-/force–response curves are used to explore the nonlinear behaviors of the system, especially the influence of vertical support stiffness, excitation frequency and amplitude on the internal resonance of the system is considered. To a certain extent, the support stiffness can reduce the response amplitudes of members by absorbing some energy from excitation.

Keywords Nonlinear vibration · Modeling · Cable-stayed bridge · Vertical support stiffness · Internal resonance

1 Introduction

As one of the popular bridges, cable-stayed bridge is of the large spanning ability, elegant appearance and mature method of construction. However, cable-stayed bridge is sensitive to external load due to its lower stiffness and the complex environments, which has been attracting many researchers [1–4]. In order to understand its internal mechanism of dynamics and find appropriate method to control its large vibration, many scholars have been devoted to researches on dynamics of the cable-stayed bridge.

To study the dynamic properties of cable-stayed bridge, a simplified model, i.e., a single cable [5–8] or a cable-stayed beam is utilized by many scholars. Fujino et al. [9] established a three-degree-of freedom model of a cable-stayed beam and the one-to-one-to-two internal resonance was observed from a theoretical and experimental point of view. Fung et al. [10] studied the nonlinear vibrations of a cable-stayed

H. Kang (✉)
College of Civil Engineering and Architecture, Guangxi University, Nanning 530004, China
e-mail: houjun_kang@163.com

H. Kang · X. Su (✉)
College of Civil Engineering, Hunan University, Changsha 410082, China
e-mail: su_xiaoyang@hnu.edu.cn

Z. Pi
China Machinery International Engineering Design & Research Institute Co., Ltd, Changsha 410021, Hunan, China

beam with time-varying length and tension in the cable by using Hamilton's principle and finite element method. Zhang et al. [11] investigated one-to-one main parametric resonance of the cable-stayed beam. In their study, the 'beat' vibration was observed and they mentioned that the occurrence of amplitude main parametric excitation resonances can be controlled by limiting the initial displacement of the beam end. Lenci and Ruzziconi [12] explored the nonlinear dynamic of a planar cable-supported beam. They pointed out that the effects of secondary attractors cannot be ignored and awakened the designer that the dynamics of cable-supported beam was complex due to resonance. Gattulli and co-workers [13–15] investigated the parametric influence on linear and nonlinear behaviors of the cable-stayed bridge. A localization factor is proposed to evaluate the localization level of cables and the nonlinear interaction between global and local modes was investigated by analytical, finite element and experimental models. They found that the axial force caused by cable tension has little influence on the natural frequencies of the cable-stayed beam even within a wide range of parameter. Wei et al. [16] studied the bifurcation and chaos of a cable-stayed beam when internal and external resonances simultaneously occur. In another paper, Wei et al. [17] analyzed the nonlinear dynamics of cable-beam coupled system driven by subharmonic resonance of the beam and principle parametric resonance of the cable. Meanwhile, the parametric analysis aiming to some key parameters of the cable-stayed beam was carried out systematically. In addition to the cable-stayed beam, there are also some models for the overall modeling of the cable-stayed bridge, such as the model consists of a simply supported four-cable-stayed deck beam and two rigid towers [18], the dynamic multi-beam model with discrete springs [19, 20] and so on.

The above cable-stayed beam model can reveal the nonlinear coupling between the cable and beam, whereas the geometric of the beam is not taken into account. In the practical engineering, a certain pre-arch value is usually set for long-span cable-stayed bridge to offset the vertical displacement caused by the shrinkage or creep of concrete during the working state of the bridge. Hence, many studies considering the initial configuration of the beam emerged. Blair et al. [21] considered the dynamic response of a shallow arch subjected to harmonic excitation by using harmonic balance method and continuation technique. The results show that a small change in excitation frequency or amplitude will lead to an obvious change in the response of the arch. Breslavsky et al. [22] investigated the stability of the snap-through of a shallow arch by utilizing a two-degree-of-freedom nonlinear model. Benedettini et al. [23] studied the nonlinear coupling and dynamic instability of a non-shallow arch. By applying theoretical and experimental methods, the post-critical behavior and two-to-one internal resonance between the first symmetric and antisymmetric modes were discussed. Recently, Kang et al. [24, 25] established a double-cable-stayed shallow-arch model of the cable-stayed bridge and studied 1:1:1 the internal resonance analysis among the shallow arch and two cables.

On the other hand, in previous studies, the boundary conditions of the model are considered to be hinged–hinged (H–H) or clamped–clamped (C–C). Actually, due to the existence of isolation rubber, the bearing may produce slight deformation, which will lead to an obvious reduction in the natural frequency of the system, especially low-order frequency [26]. Leissa and Qatu [27] considered that even a steel beam that is completely welded to an infinite constraining block (that is, an infinite half-space) will rotate at the clamping end during vibration. Yi et al. [28] proved that the elastic constraints played a significant role in the nonlinear dynamics of the elastically constrained shallow arch, which will affect the frequency and mode shape of the system. And there was a correspondence between the elastic constraints and the coefficients in the modulation equation. Hence, it is more reasonable to treat the boundary condition as elastic support and consider its stiffness, which has been adopted in many references, e.g., [28–32] to name but a few.

This paper aims to establish a more accurate model, i.e., a multi-cable-stayed shallow-arch model with vertical elastic supports at both ends, to study the nonlinear dynamics of the cable-stayed bridge. Since the initial configuration of the beam and the support stiffness of the bearing are considered, the model is closer to the real state of the cable-stayed bridge and can reflect the nonlinear phenomena in the practical engineering better. This study will explore the effect of support stiffness on the nonlinear dynamics of the cable-stayed bridge. By solving the planar eigenvalue problems of the proposed model, the mode shapes are

obtained and taken as the trial functions in Galerkin's procedure. In this way, a set of ordinary differential equations (ODEs) are derived. By utilizing the multiple time scale method, the ODEs are solved and the 1:2:2 internal resonance among the first modes of the shallow arch and two cables are explored. Meanwhile, the frequency-/force–response curves are presented to investigate the effect of support stiffness on the dynamic properties of the system.

The paper is organized as follows. In Sect. 2, the planar eigenvalue problem of the model is solved. In Sect. 3, the differential equations of the system are solved by the multiple time scale method. Numerical analysis of 1:2:2 internal resonance is performed in Sect. 4. Conclusions are given in Sect. 5.

2 Planar eigenvalue problem

The problem model considered is depicted in Fig. 1, in which $n+1$ Cartesian coordinates soy and $x_jo_jy_j$ ($j = 1, 2\ldots n$) are established to describe the motions of the shallow arch (hereinafter referred to as arch) and cables. According to the number n of cables, the arch is divided into $n+1$ segments. θ_j is the angle between the cable and the arch. v_a^* and u_a^* denote transverse and axial displacements of the arch, while v_{cj}^* and u_{cj}^* denote transverse and axial displacements of the cable. Considering the influence of bearing deformation, the vertical supports at both ends are replaced by two springs, the stiffness of which are k_1^* and k_2^*, respectively. Additionally, the arch is subjected to a harmonic excitation, i.e., $f^*\cos\Omega^* t$, which can be used to simulate wind action [33, 34]. For simplicity, the following assumptions are made:

(a) the sag-to-span ratio of the cable is small ($\leq$ 1/10). Hence, the equilibrium configuration for the inclined cable is described by the parabola [13];
(b) the initial deflection of the arch is described through a sinusoidal function and also its rise-to-span ratio f_0^* is much less than 1/10;
(c) the axial vibration of the arch is neglected, because it is usually much smaller than transverse vibration and its frequency is far more than that of transverse vibration;
(d) the displacement of the cable is considered as the superposition of two parts, i.e., pure modal displacement and vertical dragging by the vibration of the arch.
(e) the tower is considered to be rigid, since the stiffness of the tower is usually larger than that of the beam, which is also verified by experimental measurements and finite element analysis [18].

According to Hamilton's principle, the differential equations governing the planar motion of the arch segment [35] and cables [13] can be expressed as

$$m_{ai}\ddot{v}_{ai}^* + E_{ai}I_{ai}v_{ai}^{*\prime\prime\prime\prime} + \mu_{ai}^*\dot{v}_{ai}^* - \frac{1}{l_a}(y_0^{*\prime\prime} + v_{ai}^{*\prime\prime})\sum_{p=1}^{n+1} E_{ap}A_{ap}\int_{s_{p-1}^*}^{s_p^*}(y_0^{*\prime}v_{ap}^{*\prime} + \frac{1}{2}v_{ap}^{*\prime 2})\mathrm{d}s^* = p_a^*(s^*,t) \tag{1}$$

$$m_{cj}\ddot{v}_{cj}^* + \mu_{cj}^*\dot{v}_{cj}^* - [H_{cj}v_{cj}^{*\prime\prime} + E_{cj}A_{cj}(y_{cj}^{*\prime\prime} + v_{cj}^{*\prime\prime})e_j^*(t)] = 0 \tag{2}$$

where $i = 1,\ 2\ldots n+1,\ s_0^* = 0, s_{n+1}^* = l_a$ and '$*$' denotes dimensional parameter. The subscripts a and c represent the arch and the cable, respectively. m, E, I, ξ and A are mass per unit length, Young's modulus, moment of inertia of the cross section, damping parameter and cross-sectional area of the arch and

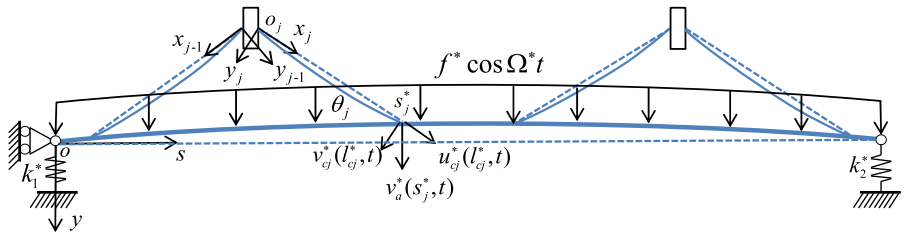

Fig. 1 Multi-cable-stayed shallow-arch model with vertical elastic supports of cable-stayed bridge

cables, respectively. y_0 and l_a are the initial configuration and horizontal length of the arch, respectively. H_{cj} and y_{cj} is the initial force and initial configuration of the jth cable, respectively. $p_a^*(s^*,t)$ is the total load acting on the arch, which will be given later. The prime and dot denote the differentiation with respect to coordinate x_j^* and time t. e_j^* denotes the uniform dynamic elongation of the cable and is given by

$$e_j^*(t)=\frac{u_{cj}^*(l_{cj},t)}{l_{cj}}+\frac{1}{l_{cj}}\int_0^{l_{cj}}(y_{cj}^{*\prime}v_{cj}^{*\prime}+\frac{1}{2}v_{cj}^{*\prime 2})\mathrm{d}x_j^* \tag{3}$$

where l_{cj} is the length of the jth cable.

For the convenience of calculation, only two cables (n = 2) are considered and the model is assumed to be symmetrical. In this case, i = 1, 2, 3 and j = 1, 2 (hereinafter inclusive). According to Fig. 1, the boundary conditions of the model can be written as

$$v_{a1}^{*\prime\prime}(0,t)=v_{a3}^{*\prime\prime}(l_a,t)=0,\quad v_{cj}^*(0,t)=0 \tag{4}$$

The continuous conditions at the node s_j^* are

$$\begin{aligned}
&v_{aj}^*(s_j^*,t)=v_{a(j+1)}^*(s_j^*,t),\ v_{aj}^{*\prime}(s_j^*,t)\\
&\quad=v_{a(j+1)}^{*\prime}(s_j^*,t),\ v_{aj}^{*\prime\prime}(s_j^*,t)=v_{a(j+1)}^{*\prime\prime}(s_j^*,t)\\
&u_{cj}^*(l_{cj},t)=v_{aj}^*(s_j^*,t)\sin\theta_j,\ v_{cj}^*(l_{cj},t)\\
&\quad=v_{aj}^*(s_j^*,t)\cos\theta_j\quad(j=1,2)
\end{aligned} \tag{5}$$

Meanwhile, the left and right side of the node s_j^* should satisfy the following mechanical relationships

$$\begin{aligned}
&E_{aj}I_{aj}v_{aj}^{*\prime\prime\prime}(s_j^*,t)-E_{a(j+1)}I_{a(j+1)}v_{a(j+1)}^{*\prime\prime\prime}(s_j^*,t)\\
&=E_{cj}A_{cj}e_j^*(t)\sin\theta_j+H_{cj}v_{cj}^{*\prime}(l_{cj},t)\cos\theta_j\\
&\quad+E_{cj}A_{cj}e_j^*(t)[v_{cj}^{*\prime}(l_{cj},t)+y_{cj}^{*\prime}(l_{cj})]\cos\theta_j
\end{aligned} \tag{6}$$

In addition, the following mechanical boundary conditions at the elastic supports can be derived through Hamilton's principle, i.e.,

$$\begin{aligned}
&E_{a1}I_{a1}v_{a1}^{*\prime\prime\prime}(0,t)+k_1^*v_{a1}^*(0,t)-[y_0^{*\prime}(0)\\
&\quad+v_{a1}^{*\prime}(0,t)]\sum_{p=1}^{3}E_{ap}A_{ap}\int_{s_{p-1}^*}^{s_p^*}(y_0^{*\prime}v_{ap}^{*\prime}+\frac{1}{2}v_{ap}^{*\prime 2})\mathrm{d}s^*\\
&\quad=0
\end{aligned} \tag{7}$$

$$\begin{aligned}
&E_{a3}I_{a3}v_{a1}^{*\prime\prime\prime}(l_a,t)-k_2^*v_{a3}^*(l_a,t)-[y_0^{*\prime}(l_a)\\
&\quad+v_{a3}^{*\prime}(l_a,t)]\sum_{p=1}^{3}E_{ap}A_{ap}\int_{s_{p-1}^*}^{s_p^*}(y_0^{*\prime}v_{ap}^{*\prime}+\frac{1}{2}v_{ap}^{*\prime 2})\mathrm{d}s^*\\
&\quad=0
\end{aligned} \tag{8}$$

Substituting Eq. (5) into Eq. (3), we can obtain

$$e_j^*(t)=\frac{v_{aj}^*(s_j^*,t)\sin\theta_j}{l_{cj}}+\frac{1}{l_{cj}}\int_0^{l_{cj}}(y_{cj}^{*\prime}v_{cj}^{*\prime}+\frac{1}{2}v_{cj}^{*\prime 2})\mathrm{d}x_j^* \tag{9}$$

To render the equations non-dimensional, the following non-dimensional variables and parameters are defined:

$$\begin{aligned}
&x_j=\frac{x_j^*}{l_{cj}},\ \tau=\omega_0 t,\ y_j=\frac{y_j^*}{l_{cj}}\ u_{cj}=\frac{u_{cj}^*}{l_{cj}},\\
&v_{cj}=\frac{v_{cj}^*}{l_{cj}},\ \lambda_{cj}=\frac{E_{cj}A_{cj}}{H_{cj}},\ v_{ai}=\frac{v_{ai}^*}{l_a},\\
&\gamma_{cj}=\frac{l_a}{l_{cj}},s=\frac{s^*}{l_a},\omega_0=1.0\mathrm{rad}\cdot\mathrm{s}^{-1},\\
&\mu_{ai}=\frac{\mu_{ai}^*}{m_{ai}\omega_0},d_j=\frac{d_j^*}{l_{cj}},y_0=\frac{y_0^*}{l_a},\mu_{cj}=\frac{\mu_{cj}^*}{m_{cj}\omega_0},\\
&\chi_j=\frac{E_{aj}I_{aj}}{l_a^2E_{cj}A_{cj}},\chi_{j+1}=\frac{E_{a(j+1)}I_{a(j+1)}}{l_a^2E_{cj}A_{cj}},\beta_{ai}^4=\frac{m_{ai}l_a^4\omega_0^2}{E_{ai}I_{ai}},\\
&\beta_{cj}^2=\frac{m_{cj}l_{cj}^2\omega_0^2}{H_{cj}},\\
&f_0=\frac{f_0^*}{l_a},\eta_{ai}=\frac{A_{ai}l_a^2}{I_{ai}},p_a=\frac{p_a^*}{m_a\omega_0^2l_a^2},k_1=\frac{k_1^*l_a^3}{E_{a1}I_{a1}},\\
&k_2=\frac{k_2^*l_a^3}{E_{a(n+1)}I_{a(n+1)}},\quad(i=1,2,3)
\end{aligned}$$

Then Eqs. (1), (2) and (9) are transformed into non-dimensional form as

$$\begin{aligned}
&\ddot{v}_{ai}+\frac{1}{\beta_{ai}^4}v_{ai}^{\prime\prime\prime\prime}+\mu_{ai}\dot{v}_{ai}-\frac{1}{\beta_{ai}^4}(y_0^{\prime\prime}\\
&\quad+v_{ai}^{\prime\prime})\sum_{p=1}^{3}\eta_{ap}\int_{s_{p-1}}^{s_p}(y_0^{\prime}v_{ap}^{\prime}+\frac{1}{2}v_{ap}^{\prime 2})\mathrm{d}s\\
&\quad=p_a(s,\tau)
\end{aligned} \tag{10}$$

$$\ddot{v}_{cj}+\mu_{cj}\dot{v}_{cj}-\frac{1}{\beta_{cj}^2}v_{cj}^{\prime\prime}-\frac{1}{\beta_{cj}^2}\lambda_{cj}e_j(y_{cj}^{\prime\prime}+v_{cj}^{\prime\prime})=0 \tag{11}$$

$$e_j(\tau) = -\gamma_{cj} v_{aj}(s_j,\tau)\sin\theta_j + \int_0^1 \left(y'_{cj}v'_{cj} + \frac{1}{2}v'^2_{cj}\right)\mathrm{d}x_j \tag{12}$$

To solve the planar eigenvalue problem of the model, the excitation, nonlinear and damping terms of Eqs. (10) and (11) are commonly ignored, then we can obtain

$$\ddot{v}_{ai} + \frac{1}{\beta_{ai}^4}v''''_{ai} - \frac{1}{\beta_{ai}^4}y''_0\sum_{p=1}^{3}\eta_{ap}\int_{s_{p-1}}^{s_p} y'_0 v'_{ap}\mathrm{d}s = 0 \tag{13}$$

$$\ddot{v}_{cj} - \frac{1}{\beta_{cj}^2}v''_{cj} - \frac{1}{\beta_{cj}^2}\lambda_{cj}\hat{e}_j y''_{cj} = 0 \tag{14}$$

where

$$\hat{e}_j = v_{cj}(1,\tau)\tan\theta_j + \int_0^1 y'_{cj}v'_{cj}\mathrm{d}x_j \tag{15}$$

The non-dimensional linear forms of Eqs. (4)–(8) can be written as

$$v''_{a1}(0,\tau) = v''_{a3}(1,\tau) = 0, \quad v_{cj}(0,\tau) = 0 \tag{16}$$

$$\begin{aligned} v_{aj}(s_j,\tau) &= v_{a(j+1)}(s_j,\tau), v'_{aj}(s_j,\tau) = v'_{a(j+1)}(s_j,\tau),\\ &\quad v''_{aj}(s_j,\tau) = v''_{a(j+1)}(s_j,\tau)\\ u_{cj}(1,\tau) &= \gamma_{cj}v_{aj}(s_j,\tau)\sin\theta_j, v_{cj}(1,\tau)\\ &= \gamma_{cj}v_{aj}(s_j,\tau)\cos\theta_j \end{aligned} \tag{17}$$

$$\begin{aligned} &\chi_j v''''_{aj}(s_j,\tau) + \chi_{j+1}v''''_{a(j+1)}(s_j,\tau)\\ &= \hat{e}_j(\tau)\sin\theta_j + \frac{\cos\theta_j}{\lambda_{cj}}v'_{cj}(1,\tau) + \hat{e}_j(t)y'_{cj}(1)\cos\theta_j \end{aligned} \tag{18}$$

$$\begin{aligned} &v'''_{a1}(0,\tau) + k_1 v_{a1}(0,\tau) - y'_0(0)\sum_{p=1}^{3}\eta_{ap}\int_{s_{p-1}}^{s_p} y'_0 v'_{ap}\mathrm{d}s\\ &= 0 \end{aligned} \tag{19}$$

$$\begin{aligned} &v'''_{a3}(1,\tau) - k_2 v_{a3}(1,\tau) - y'_0(1)\sum_{p=1}^{3}\eta_{ap}\int_{s_{p-1}}^{s_p} y'_0 v'_{ap}\mathrm{d}s\\ &= 0 \end{aligned} \tag{20}$$

The solutions of Eqs. (13) and (14) can be expressed as

$$v_{ai} = \phi_{ai}(s)e^{i(\omega/\omega_0)\tau} \quad v_{cj} = \phi_{cj}(x)e^{i(\omega/\omega_0)\tau} \tag{21}$$

According to assumptions (a) and (b), the initial configurations of cables are expressed as

$$y_{cj}(x_j) = 4d_j(x_j - x_j^2) \tag{22}$$

where d_j is the sag-to-span ratio of the cable.

Substituting Eqs. (21) and (22) into Eqs. (13) and (14), we can obtain

$$\phi''''_{ai} - \overline{\beta}_a^4\phi_{ai} = \eta_a y''_0\sum_{p=1}^{3}\int_{s_{p-1}}^{s_p} y'_0\phi'_{ap}\mathrm{d}s \tag{23}$$

$$\overline{\beta}_c^2\phi_{cj} + \phi''_{cj} = 8\lambda_c d\hat{e}_j \tag{24}$$

where $\overline{\beta}_a^4 = \frac{m_a l_a^4\omega^2}{E_a I_a}$, $\overline{\beta}_c^2 = \frac{m_c l_c^2\omega^2}{H_c}$ and

$$\hat{e}_j = \phi_{cj}(1)\tan\theta_j + \int_0^1 y'_{cj}\phi'_{cj}\mathrm{d}x_j \tag{25}$$

Substituting Eq. (21) into Eqs. (16)–(20), the following can be derived

$$\phi''_{a1}(0) = \phi''_{a3}(1) = 0, \quad \phi_{cj}(0) = 0 \tag{26}$$

$$\begin{aligned} \phi_{aj}(s_j) &= \phi_{a(j+1)}(s_j), \ \phi'_{aj}(s_j) = \phi'_{a(j+1)}(s_j), \ \phi''_{aj}(s_j)\\ &= \phi''_{a(j+1)}(s_j), \ \phi_{cj}(1) = \gamma_{cj}\phi_{aj}(s_j)\cos\theta_j \end{aligned} \tag{27}$$

$$\begin{aligned} \chi_j\phi'''_{aj}(s_j) + \chi_{j+1}\phi'''_{a(j+1)} &= \hat{e}_j(\tau)\sin\theta_j + \frac{\cos\theta_j}{\lambda_{cj}}\phi'_{cj}(1)\\ &\quad + \hat{e}_j(t)y'_{cj}(1)\cos\theta_j \end{aligned} \tag{28}$$

$$\phi'''_{a1}(0) + k_1\phi_{a1}(0) - y'_0(0)\sum_{p=1}^{3}\eta_{ap}\int_{s_{p-1}}^{s_p} y'_0\phi'_{ap}\mathrm{d}s = 0 \tag{29}$$

$$\phi'''_{a3}(1) - k_2\phi_{a3}(1) - y'_0(1)\sum_{p=1}^{3}\eta_{ap}\int_{s_{p-1}}^{s_p} y'_0\phi'_{ap}\mathrm{d}s = 0 \tag{30}$$

The general solution of Eq. (24) is

$$\phi_{cj}(x) = c_{j1}\sin\overline{\beta}_c x + c_{j2}\cos\overline{\beta}_c x + D_{jc} \tag{31}$$

where

$$D_{jc} = \frac{8\lambda_c d\hat{e}_j}{\overline{\beta}_c^2} \tag{32}$$

According to Eqs. (25) and (32), we can derive

$$D_{jc} = \eta_{j1}c_{j1} + \eta_{j2}c_{j2} \tag{33}$$

where

$$\eta_{j1} = \frac{8\lambda_c d}{\overline{\beta}_c^2 - 8\lambda_c d\tan\theta_j} \times \left[\sin\overline{\beta}_c\tan\theta_j - 4d(\sin\overline{\beta}_c + \frac{2\cos\overline{\beta}_c - 2}{\overline{\beta}_c})\right]$$

$$\eta_{j2} = \frac{8\lambda_c d}{\overline{\beta}_c^2 - 8\lambda_c d\tan\theta_j} \times \left[\cos\overline{\beta}_c\tan\theta_j - 4d(1 + \cos\overline{\beta}_c - \frac{2\sin\overline{\beta}_c}{\overline{\beta}_c})\right]$$

The general solution of Eq. (23) is

$$\phi_{ai}(s) = a_{i1}\cos\overline{\beta}_a s + a_{i2}\sin\overline{\beta}_a s + a_{i3}\cosh\overline{\beta}_a s + a_{i4}\sinh\overline{\beta}_a s + a_{i5}h \tag{34}$$

where h belongs to particular solution, which can be chosen as $h = \sin\pi s$.

Obviously, Eq. (34) has to satisfy Eq. (13). Together with Eqs. (26)–(30), we finally obtain the following equation

$$[\boldsymbol{T}]\{\boldsymbol{X}\} = 0 \tag{35}$$

where $\{\boldsymbol{X}\}=\{c_{j1},c_{j2},a_{i1},a_{i2},a_{i3},a_{i4},a_{i5}\}^{\mathrm{T}}$. The elements of the matrix $[\boldsymbol{T}]$ in Eq. (35) are reported in "Appendix A". Equation (35) is just so-called characteristic equation of the system, which is the function of natural frequencies. Using numerical analysis software, the frequencies and mode shapes can be obtained.

3 Perturbation technique

In this section, the nonlinear analysis of the model is performed. Here, there is no need to segment the shallow arch, because the interaction between the cable and arch is illustrated by external load (see Eq. (37)) and excitation (see Eq. (39)). In this case, the non-dimensional form of the differential equations governing the planar motion of the arch can be written as

$$\ddot{v}_a + \frac{1}{\beta_a^4}v_a'''' + \mu_a\dot{v}_a - \frac{\eta_a}{\beta_a^4}\left(v_a'' + y_0''\right)\left[\int_0^1\left(\frac{1}{2}v_a'^2 + y_0'v_a'\right)\mathrm{d}s\right] = p_a(s,\tau) \tag{36}$$

where $p_a(s,\tau)$ consists of two parts, namely, the action of the cable and the external load. It can be expressed by

$$p_a(s,\tau) = \sum_{j=1}^{2}\delta(s - s_j)K_j e_j(\tau)\sin\theta_j \quad (j = 1,2) \tag{37}$$

where $K_j = \frac{E_{cj}A_{cj}}{m_a\omega_0^2 l_a^2}$, $f = \frac{f^*}{m_a\omega_0^2 l_a}$ and $\Omega = \frac{\Omega^*}{\omega_0}$. $\delta()$ denotes Kronecker delta function.

Based on the assumption (d), the non-dimensional forms of the planar transverse displacements of the arch and cables are expressed as

$$v_a(s,\tau) = \phi_a(s)g(\tau) \tag{38}$$

$$v_{cj}(x_j,\tau) = \gamma_{cj}v_a(s,\tau)x_j\cos\theta_j + \phi_{cj}(x_j)q_j(\tau) \tag{39}$$

where $g(\tau)$ and $q_j(\tau)$ are generalized coordinates. $\phi_a(x)$ is the modal function of the arch, which is determined in Sec. 2. $\phi_{cj}(x_j)$ is the pure modal function of cables and are taken as sinusoidal function for simplicity. Substituting Eqs. (38) and (39) into Eqs. (36) and (11) and applying Galerkin's method, the following ODEs can be derived

$$\ddot{g} + \mu_a\dot{g} + b_{11}g + b_{12}g^2 + b_{13}g^3 + b_{14}q_1 + b_{15}gq_1 + b_{16}q_2 + b_{17}gq_2 + b_{18}q_1^2 + b_{19}q_2^2 + b_{110}\cos(\Omega\tau) = 0 \tag{40}$$

$$\ddot{q}_j + \mu_{cj}\dot{q}_j + b_{(j+1)1}\dot{g} + b_{(j+1)2}\ddot{g} + b_{(j+1)3}g + b_{(j+1)4}q_j + b_{(j+1)5}g^2 + b_{(j+1)6}gq_j + b_{(j+1)7}q_j^2 + b_{(j+1)8}g^2q_j + b_{(j+1)9}gq_j^2 + b_{(j+1)10}q_j^3 = 0 \tag{41}$$

where j = 1,2. b_{mo} (m = 1,2,3 and o = 1,2…10) are Galerkin's integral coefficients and they are presented in "Appendix B". Next, the multiple time scale method is applied to solve Eqs. (40) and (41). First, a small bookkeeping parameter ε is introduced, namely

$$\begin{aligned}
&\varepsilon^2\tilde{\mu}_a=\mu_a, \varepsilon\tilde{b_{12}}=b_{12}, \varepsilon^2\tilde{b_{13}}=b_{13}, \varepsilon\tilde{b_{14}}=b_{14},\\
&\varepsilon\tilde{b_{15}}=b_{15}, \varepsilon\tilde{b_{16}}=b_{16}, \varepsilon\tilde{b_{17}}=b_{17}, \varepsilon\tilde{b_{18}}=b_{18},\\
&\varepsilon\tilde{b_{19}}=b_{19}, \varepsilon^2\tilde{b_{110}}=b_{110}\\
&\varepsilon^2\tilde{\mu}_{cj}=\mu_{cj}, \varepsilon^2\tilde{b}_{(j+1)1}=b_{(j+1)1}, \varepsilon^2\tilde{b}_{(j+1)2}=b_{(j+1)2},\\
&\varepsilon\tilde{b}_{(j+1)3}=b_{(j+1)3},\\
&\varepsilon\tilde{b}_{(j+1)5}=b_{(j+1)5}, \varepsilon\tilde{b}_{(j+1)6}=b_{(j+1)6}, \varepsilon\tilde{b}_{(j+1)7}=b_{(j+1)7}\\
&\varepsilon^2\tilde{b}_{(j+1)8}=b_{(j+1)8}, \varepsilon^2\tilde{b}_{(j+1)9}=b_{(j+1)9}, \varepsilon^2\tilde{b}_{(j+1)10}=b_{(j+1)10}
\end{aligned}$$

To balance the damping, excitation and nonlinear terms, Eqs. (40) and (41) are rewritten as

$$\begin{aligned}
&\ddot{g}+\varepsilon^2\mu_a\dot{g}+\omega_a^2 g+\varepsilon b_{12}g^2+\varepsilon^2 b_{13}g^3+\varepsilon b_{14}q_1\\
&+\varepsilon b_{15}gq_1+\varepsilon b_{16}q_2+\varepsilon b_{17}gq_2+\varepsilon b_{18}q_1^2+\varepsilon b_{19}q_2^2\\
&+\varepsilon^2 b_{110}\cos(\Omega\tau)=0
\end{aligned} \tag{42}$$

$$\begin{aligned}
&\ddot{q}_j+\varepsilon^2\mu_{cj}\dot{q}_j+\varepsilon^2 b_{(j+1)1}\dot{g}+\varepsilon^2 b_{(j+1)2}\ddot{g}+\varepsilon b_{(j+1)3}g\\
&+\omega_j^2 q_j+\varepsilon b_{(j+1)5}g^2+\varepsilon b_{(j+1)6}gq_j+\varepsilon b_{(j+1)7}q_j^2\\
&+\varepsilon^2 b_{(j+1)8}g^2q_j\\
&+\varepsilon^2 b_{(j+1)9}gq_j^2+\varepsilon^2 b_{(j+1)10}q_j^3=0
\end{aligned} \tag{43}$$

where the wavy symbols on the letters have been removed for brevity and $\omega_a^2=b_{11}, \omega_1^2=b_{24}, \omega_2^2=b_{34}$.

To obtain a second order approximation, a fast time scale $T_0=\varepsilon^0\tau$ and a slow time scale $T_2=\varepsilon^2\tau$ are introduced, respectively. In this way, the solutions of g and q_j are uniformly expanded in power series of ε as

$$\begin{aligned}
g&=\sum_{i=1}^{3}\varepsilon^{i-1}g_i(T_0,T_2)+O(\varepsilon^3),\\
q_j&=\sum_{i=1}^{3}\varepsilon^{i-1}q_{ji}(T_0,T_2)+O(\varepsilon^3)
\end{aligned} \tag{44}$$

Substituting Eq. (44) into Eqs. (42) and (43) and equating the terms of like order in ε, we can obtain.

order ε^0,

$$\begin{aligned}
&(D_0^2+\omega_a^2)g_1=0\\
&(D_0^2+\omega_j^2)q_{j1}=0
\end{aligned} \tag{45}$$

order ε^1,

$$\begin{aligned}
&(D_0^2+\omega_a^2)g_2=\\
&-(b_{12}g_1^2+b_{14}q_{11}+b_{15}g_1q_{11}+b_{16}q_{21}+b_{17}g_1q_{21}+b_{18}q_{11}^2+b_{19}q_{21}^2)\\
&(D_0^2+\omega_j^2)q_{j2}=\\
&-(b_{(j+1)3}g_1+b_{(j+1)5}g_1^2+b_{(j+1)6}g_1q_{j1}+b_{(j+1)7}q_{j1}^2)
\end{aligned} \tag{46}$$

order ε^2,

$$\begin{aligned}
&(D_0^2+\omega_a^2)g_3=\\
&-(\mu_aD_0^1g_1+2D_0^1D_2^1g_1+2b_{12}g_1g_2+b_{13}g_1^3\\
&+b_{14}q_{12}+b_{15}g_1q_{12}+b_{15}g_2q_{11}+b_{16}q_{22}\\
&+b_{17}g_1q_{22}+b_{17}g_2q_{21}+2b_{18}q_{11}q_{12}+2b_{19}q_{21}q_{22}\\
&+b_{110}\cos(\Omega T_0))\\
&(D_0^2+\omega_j^2)q_{j3}=\\
&-(b_{(j+1)1}D_0^1g_1+b_{(j+1)2}D_0^2g_1+\mu_{cj}D_0^1q_{j1}\\
&+2D_0^1D_2^1q_{j1}+b_{(j+1)3}g_2+2b_{(j+1)5}g_1g_2\\
&+b_{(j+1)6}g_1q_{j2}+b_{(j+1)6}g_2q_{j1}+2b_{(j+1)7}q_{j1}q_{j2}\\
&+b_{(j+1)8}g_1^2q_{j1}+b_{(j+1)9}g_1q_{j1}^2+b_{(j+1)10}q_{j1}^3)
\end{aligned} \tag{47}$$

where D_w^j is a differential operator and it is defined as $D_w^j=\partial^j/\partial T_w$ (j = 1,2 and w = 0,2).

The solutions of Eq. (45) is

$$g_1=A_1(T_2)\exp(\mathrm{i}\omega_aT_0)+cc \tag{48}$$

$$q_{j1}=A_{j+1}(T_2)\exp(\mathrm{i}\omega_jT_0)+cc \tag{49}$$

where cc denotes the complex conjugates of the preceding terms. $A_m(T_2)$ are the complex amplitudes, which will be determined by eliminating the secular terms in the following. Substituting Eqs. (48) and (49) into Eq. (46), and ignoring the homogenous solutions, we can obtain the solutions of Eq. (46). In order to study one-to-two-to-two internal resonance of the system, substituting the solutions of Eq. (46) into Eq. (47) together with Eqs. (48) and (49), the following can be derived

$$
\begin{aligned}
&(D_0^2+\omega_a^2)g_3\\
&=-\frac{1}{2}b_{110}\exp(\mathrm{i}T_0\Omega)-\mathrm{i}\mu_a\omega_a A_1\exp(\mathrm{i}T_0\omega_a)\\
&\quad-2\mathrm{i}\omega_a D_2^1A_1\exp(\mathrm{i}T_0\omega_a)+\Gamma_a^1A_1^2B_1\exp(\mathrm{i}T_0\omega_a)\\
&\quad+\Gamma_a^2A_1\exp(\mathrm{i}T_0\omega_a)+\Gamma_a^3A_1A_2B_2\exp(\mathrm{i}T_0\omega_a)\\
&\quad+\Gamma_a^4A_1A_3B_3\exp(\mathrm{i}T_0\omega_a)+\Gamma_a^5A_2B_1\exp\mathrm{i}T_0(\omega_b-\omega_a)\\
&\quad+\Gamma_a^6A_3B_1\exp(\omega_c-\omega_a)\\
&\quad+\Gamma_a^7A_1A_3B_2\exp\mathrm{i}T_0(\omega_a-\omega_b+\omega_c)\\
&\quad+\Gamma_a^8A_1A_2B_3\exp\mathrm{i}T_0(\omega_a+\omega_b-\omega_c)+NST_1+cc
\end{aligned}
\tag{50}
$$

$$
\begin{aligned}
&(D_0^2+\omega_b^2)q_{13}\\
&\quad=-\mathrm{i}\mu_{c1}\omega_bA_2\exp(\mathrm{i}T_0\omega_b)-2\mathrm{i}\omega_bD_2^1A_2\exp(\mathrm{i}T_0\omega_b)\\
&\quad+\Gamma_b^1A_1A_2B_1\exp(\mathrm{i}T_0\omega_b)+\Gamma_b^2A_2^2B_2\exp(\mathrm{i}T_0\omega_b)\\
&\quad+\Gamma_b^3A_2\exp(\mathrm{i}T_0\omega_b)+\Gamma_b^4A_2A_3B_3\exp(\mathrm{i}T_0\omega_b)\\
&\quad+\Gamma_b^5A_1^2\exp(2\mathrm{i}T_0\omega_a)+\Gamma_b^6A_3\exp(\mathrm{i}T_0\omega_c)\\
&\quad+\Gamma_b^7A_1A_3B_1\exp(\mathrm{i}T_0\omega_c)\\
&\quad+\Gamma_b^8A_3^2B_2\exp(\mathrm{i}T_0(2\omega_c-\omega_b))+NST_2+cc
\end{aligned}
\tag{51}
$$

$$
\begin{aligned}
&(D_0^2+\omega_c^2)q_{23}\\
&\quad=-\mathrm{i}\mu_{c2}\omega_cA_3\exp(\mathrm{i}T_0\omega_c)-2\mathrm{i}\omega_cD_2^1A_3\exp(\mathrm{i}T_0\omega_c)\\
&\quad+\Gamma_c^1A_1A_3B_1\exp(\mathrm{i}T_0\omega_c)+\Gamma_c^2A_3^2B_3\exp(\mathrm{i}T_0\omega_c)\\
&\quad+\Gamma_c^3A_3\exp(\mathrm{i}T_0\omega_c)+\Gamma_c^4A_2A_3B_2\exp(\mathrm{i}T_0\omega_c)\\
&\quad+\Gamma_c^5A_1^2\exp(2\mathrm{i}T_0\omega_a)+\Gamma_c^6A_2\exp(\mathrm{i}T_0\omega_b)
\end{aligned}
\tag{52}
$$

where $\omega_1=\omega_b$ and $\omega_2=\omega_c$. $B_m(T_2)$ are complex conjugates of $A_m(T_2)$. NST_m denotes non-secular terms and Γ_a^z, Γ_b^z and $\Gamma_c^z(z=1,2...8)$ are reported in "Appendix C". The nearness of the three in-plane frequencies involved in a one-to-two-to-two internal resonance is described by introducing internal and external detuning parameters σ_1, σ_2 and σ, namely

$$
\Omega=\omega_a+\varepsilon^2\sigma,\omega_b=2\omega_a+\varepsilon^2\sigma_1,\omega_c=2\omega_a+\varepsilon^2\sigma_2 \tag{53}
$$

To solve Eqs. (50)–(52), the polar forms of $A_m(T_2)$ are utilized, i.e.,

$$
A_m(T_2)=\frac{1}{2}a_m(T_2)e^{i\psi_m(T_2)} \tag{54}
$$

where $a_m(T_2)$ and $\psi_m(T_2)$ are amplitude and phase angle of $A_m(T_2)$. Substituting Eq. (54) into Eqs. (50)–(52), letting the secular terms equal to zero and separating the real and imaginary parts, the following autonomous modulation equations can be derived

$$
\begin{aligned}
8\omega_a\dot{a}_1=&-4\mu_a\omega_aa_1-4b_{110}\sin\alpha_1+2\Gamma_a^5a_1a_2\sin\alpha_2\\
&-\Gamma_a^7a_1a_2a_3\sin(\alpha_2-\alpha_3)\\
&+\Gamma_a^8a_1a_2a_3\sin(\alpha_2-\alpha_3)+2\Gamma_a^6a_1a_3\sin\alpha_3
\end{aligned}
\tag{55}
$$

$$
\begin{aligned}
8\omega_aa_1\dot{\alpha}_1=&\,8\omega_aa_1\sigma+4\Gamma_a^2a_1+\Gamma_a^1a_1^3+\Gamma_a^3a_1a_2^2+\Gamma_a^4a_1a_3^2\\
&-4b_{110}\cos\alpha_1+2\Gamma_a^5a_1a_2\cos\alpha_2\\
&+\Gamma_a^7a_1a_2a_3\cos(\alpha_2-\alpha_3)\\
&+\Gamma_a^8a_1a_2a_3\cos(\alpha_2-\alpha_3)+2\Gamma_a^6a_1a_3\cos\alpha_3
\end{aligned}
\tag{56}
$$

$$
\begin{aligned}
8\omega_b\dot{a}_2=&-4\mu_{c1}\omega_ba_2-2\Gamma_b^5a_1^2\sin\alpha_2\\
&-\Gamma_b^8a_2a_3^2\sin2(\alpha_2-\alpha_3)-4\Gamma_b^6a_3\sin(\alpha_2-\alpha_3)\\
&-\Gamma_b^7a_1^2a_3\sin(\alpha_2-\alpha_3)
\end{aligned}
\tag{57}
$$

$$
\begin{aligned}
8\omega_a\omega_ba_1a_2\dot{\alpha}_2=&\,8\omega_a\omega_ba_1a_2\sigma_1+8\Gamma_a^2a_1a_2\omega_b\\
&+2\Gamma_a^1a_1^3a_2\omega_b+2\Gamma_a^3a_1a_2^3\omega_b\\
&+2\Gamma_a^4a_1a_2a_3^2\omega_b-8a_2b_{110}\omega_b\cos\alpha_1\\
&+4\Gamma_a^5a_1a_2^2\omega_b\cos\alpha_2\\
&+2\Gamma_a^7a_1a_2^2a_3\omega_b\cos(\alpha_2-\alpha_3)\\
&+2\Gamma_a^8a_1a_2^2a_3\omega_b\cos(\alpha_2-\alpha_3)\\
&+4\Gamma_a^6a_1a_2a_3\omega_b\cos\alpha_3\\
&-4\Gamma_b^3a_1a_2\omega_a-\Gamma_b^1a_1^3a_2\omega_a\\
&-\Gamma_b^2a_1a_2^3\omega_a-\Gamma_b^4a_1a_2a_3^2\omega_a\\
&-2\Gamma_b^5a_1^3\omega_a\cos\alpha_2\\
&-\Gamma_b^8a_1a_2a_3^2\omega_a\cos2(\alpha_2-\alpha_3)\\
&-4\Gamma_b^6a_1a_3\omega_a\cos(\alpha_2-\alpha_3)\\
&-\Gamma_b^7a_1^3a_3\omega_a\cos(\alpha_2-\alpha_3)
\end{aligned}
\tag{58}
$$

$$
\begin{aligned}
8\omega_c\dot{a}_3 = & -4\mu_{c2}\omega_c a_3 + \Gamma_c^8 a_2^2 a_3 \sin 2(\alpha_2-\alpha_3) \\
& + 4\Gamma_c^6 a_2 \sin(\alpha_2-\alpha_3) + \Gamma_c^7 a_1^2 a_2 \sin(\alpha_2-\alpha_3) \\
& - 2\Gamma_c^5 a_1^2 \sin\alpha_3
\end{aligned} \tag{59}
$$

$$
\begin{aligned}
8\omega_a\omega_c a_1 a_3\dot{\alpha}_3 = & \, 8\omega_a\omega_c a_1 a_3\sigma_2 + 8\Gamma_a^2 a_1 a_3\omega_c \\
& + 2\Gamma_a^1 a_1^3 a_3\omega_c + 2\Gamma_a^3 a_1 a_2^2 a_3\omega_c \\
& + 2\Gamma_a^4 a_1 a_3^3\omega_c - 8a_3 b_{110}\omega_c\cos\alpha_1 \\
& + 4\Gamma_a^5 a_1 a_2 a_3\omega_c\cos\alpha_2 \\
& + 2\Gamma_a^7 a_1 a_2 a_3^2\omega_c\cos(\alpha_2-\alpha_3) \\
& - 2\Gamma_c^5 a_1^3\cos\alpha_3 \\
& + 2\Gamma_a^8 a_1 a_2 a_3^2\omega_c\cos(\alpha_2-\alpha_3) \\
& + 4\Gamma_a^6 a_2 a_3^2\omega_c\cos\alpha_3 - 4\Gamma_c^3 a_1 a_3\omega_a \\
& - \Gamma_c^1 a_1^3 a_3\omega_a - \Gamma_c^4 a_1 a_2^2 a_3\omega_a \\
& - \Gamma_c^2 a_1 a_3^3\omega_a \\
& - \Gamma_c^8 a_1 a_2^2 a_3\omega_a\cos 2(\alpha_2-\alpha_3) \\
& - 4\Gamma_c^6 a_1 a_2\cos(\alpha_2-\alpha_3) \\
& - \Gamma_c^7 a_1^3 a_2\omega_a\cos(\alpha_2-\alpha_3)
\end{aligned} \tag{60}
$$

where $\alpha_1 = T_2\sigma - \psi_1(T_2), \alpha_2 = T_2\sigma_1 - 2\psi_1(T_2) + \psi_2(T_2), \alpha_3 = T_2\sigma_2 - 2\psi_1(T_2) + \psi_3(T_2)$.

Letting $\dot{a}_1 = \dot{a}_2 = \dot{a}_3 = \dot{\alpha}_1 = \dot{\alpha}_2 = \dot{\alpha}_3 = 0$, the steady-state equilibrium solutions of Eqs. (55)–(60) can be obtained by Newton–Raphson method and pseudo-arclength algorithm [36]. The stability of the equilibrium solutions can be determined by checking the eigenvalues of Jacobian matrix of the system and evaluating whether the real part of each eigenvalue is negative or not [37].

Table 1 Key parameters of the arch and cables

Arch		Cables		
β_a	η_a	K_j	λ_{cj}	β_{cj}
5.69801	149,694	0.332659	1317.33	0.37238

4 Numerical analysis of 1:2:2 internal resonance

The following parameters are chosen for numerical analysis. For the arch, the length of each segment is 100 m and the total length is 300 m; mass per unit length is 4.4×10^4 kg/m; Young's modulus is 34.5Gpa; moment of inertia of the cross section is 9.8m^4; damping parameter is 0.003 and cross-sectional area is 16.3 m^2. For cables, the total length is 115.5 m; mass per unit length is 10.4 kg/m; Young's modulus is 210Gpa; damping parameter is 0.003; cross-sectional area is 6.3×10^{-3}m^2; the initial force is 1MN; the angle between the cable and arch is 30°. Additionally, the initial configuration of the arch is $y_0(s) = f_0\sin(\pi s)$ and f_0 is sag-to-span ratio of the arch, which can be used to adjust the frequencies of the arch to satisfy different internal resonance relationships. According to the above parameters, the values of some key variables are given in Table 1. Figure 2 shows the mode shapes of the arch with different support stiffness when the 1:2:2 internal resonance occurs. It can be seen that when the support stiffness is different, the mode shapes of the arch under 1:2:2 internal resonance are fundamentally changed, which indicates that the support stiffness affects the mode shapes of the arch and further affects the nonlinear behaviors of the system. Hence, in order to explore the effect of the elastic support on the nonlinear dynamics of the system, different cases of the support stiffness are considered in the following analysis. It should be noted that in the following figures, SN and HB denote saddle-node bifurcation and Hopf bifurcation, respectively. Stable solutions are represented by solid lines,

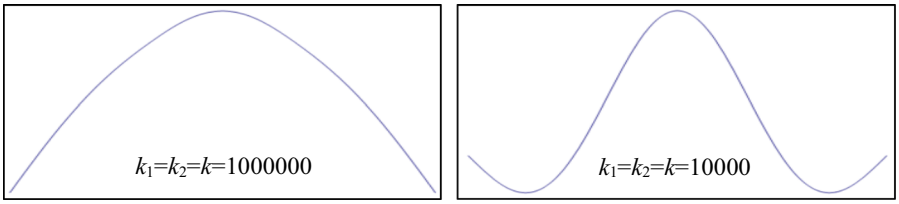

Fig. 2 The mode shapes of the arch with different support stiffness when the 1:2:2 internal resonance occurs

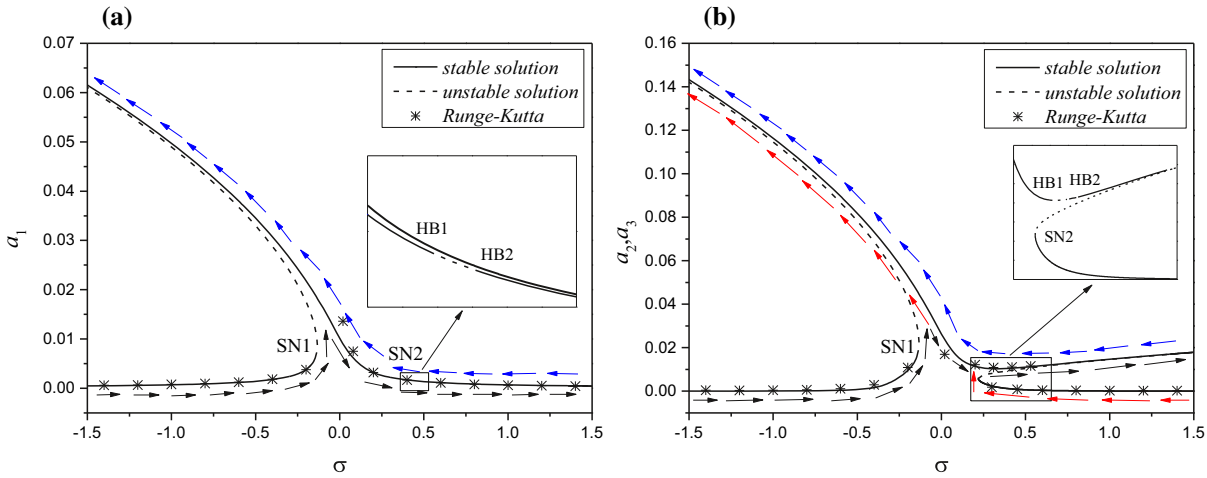

Fig. 3 The frequency–response curves of the arch and cables with $k_1 = k_2 = k = 1{,}000{,}000$, $\sigma_1 = \sigma_2 = 6.38 \times 10^{-6}$ and excitation amplitude $f = 0.001$: **a** for arch, **b** for cables

while unstable solutions are represented by dashed lines.

Firstly, in order to study the nonlinear dynamics of the system and compare it with the earlier work, relatively large support stiffness is chosen, namely, $k_1 = k_2 = k = 1{,}000{,}000$. In this case, the boundary conditions are close to H–H ends. Adjust f_0 to 0.0492 so that $2\omega_a \approx \omega_b \approx \omega_c$. Figure 3 presents the frequency–response curves of the arch and cables when excitation amplitude $f = 0.001$ and internal detuning parameters $\sigma_1 = \sigma_2 = 6.38 \times 10^{-6}$. Runge–Kutta method is also used to directly integrate Eqs. (40) and (41) in Fig. 3 and a satisfactory agreement between the two methods can be observed. It should be pointed out that the numerical results, especially the large response amplitudes, are very sensitive to the initial conditions of the system and they are relatively hard to obtain unless the initial condition is chosen precisely [38]. It can be seen from Fig. 3a that the curve of the arch (i.e., a_1) bends to the left and exhibits softening characteristic. When the excitation frequency (i.e., σ) increases from a relatively small value, the response amplitude of the arch increases slowly until SN1 is reached. If we continually increase σ, a jump from the lower branch to the upper branch will occur, as shown by the arrows in Fig. 3. After SN1, the response amplitude will decrease with the increase in σ and losses its stability via HB1, while regain stability via HB2. When $\sigma > 0.245$, there are two close branches in the response curve of the arch, which corresponds to the upper and lower branches of the response curve of the cable, respectively. This is actually related to double-jumping phenomenon [24, 25] and also confirmed in Fig. 3b. As seen in Fig. 3b, there are two peaks in the response curves and they bend to the left and right, respectively. Nayfeh et al. [39] firstly observed the double-jumping phenomenon in pitch and roll coupling vibration of a ship by a two-degree-of-freedom nonlinear model and since then, this phenomenon has been found in many other nonlinear systems.

Comparing Fig. 3(a) with Fig. 3(b), we can see that the response amplitude of the arch is smaller than that of the cable. The reason may be that the mass of the cable is much less than that of the arch and the arch provides a parametric and forced excitation at the lower end of the cable, which is consistent with the large amplitude vibration of the cable in practical engineering. Due to the existence of the double-jumping phenomenon, there are two stable solutions when $\sigma < 0.241$ or $\sigma > 0.43$ and they belong to upper and lower branches, respectively. This means that cables may exhibit different dynamic characteristics even they are subjected to the same excitation, which depends on initial conditions. This may be caused by different energy transfer mechanism, namely, the energy transferred from the arch into two cables is different at this time. Additionally, it can be found that when σ decreases from a larger value, the jumping phenomenon of the arch is different from that of the cable. The response amplitude of the cable jumps from the lower branch to the upper branch at SN2, while it is

opposite for the arch. The above phenomena are similar to those in references [24, 25], which further verifies the present model.

Figure 4 is the frequency–response curves of the arch and cables when $f = 0.002$ and $f = 0.004$. It can be seen that Fig. 4 differs a lot from Fig. 3. Compared with Fig. 3a, SN and unstable solutions of the lower branch when $\sigma > 0$ disappear in Fig. 4a. Instead, a new stable branch appears, the amplitude of which is much larger than that of the other branches. Due to the disappearance of SN on the right, the double-jumping phenomenon also vanished. This indicates that when the excitation amplitude increases to a certain value, the dynamic characteristics of the arch and cables will change. When $\sigma < 0.25$, the amplitude of the new stable branch decreases rapidly with the increase of the excitation frequency, while it is almost unchanged for cables (see Fig. 4b). This is related to the energy transfer between the arch and cables. When $\sigma < 0.25$, the arch requires a great deal of energy to maintain its large amplitude vibration, with no excess energy transferred to the cable. Hence, the response amplitude of cables is small and almost invariable for the new stable branch. This new phenomenon may exist in the earlier work but it is firstly observed in the present work.

Figure 5 illustrates the force–response curves of the arch and cables when external detuning parameter $\sigma = -0.6$. It can be seen that the jumping phenomenon occurs again. With the increase in excitation amplitudes, the response amplitudes increase rapidly until SN1 is reached. At this time, a jump from the lower branch to the upper branch will occur. If we go on increasing excitation amplitudes, the response amplitudes will increase accordingly. Inversely, if the excitation amplitudes decrease from a relatively large value, a jump from the upper branch to the lower branch triggered by SN2 will occur. However, the dynamic characteristic of the system is relatively simple when $\sigma = 0$ (see Fig. 6). There is a nonlinear relationship between the response amplitudes and the excitation amplitudes. This may be because the nonlinear terms in Eqs. (40) and (41) dominates the motion. Figure 7 shows the force–response curves of the arch and cables when external detuning parameter $\sigma = 0.6$. As seen in the figure, the dynamic behaviors of the system are considerably complex. There are three branches of unstable solutions and one stable solution. With the increase in excitation amplitude, the stable solution is almost linearly increasing and it losses its stability via HB1, while regain stability via HB2. Additionally, the dynamic behaviors of the arch and cables are similar when $\sigma = 0$ and $\sigma = 0.6$. The reason may be that there are many similar terms in the ODEs of the arch and cables as shown in Eqs. (40) and (41).

In practical engineering, even if two cables with the same parameters are symmetrically anchored on the cable-stayed bridge, the frequencies of the two cables are not exactly the same due to installation and stress redistribution. In order to study the influence of frequency difference on dynamic characteristics of

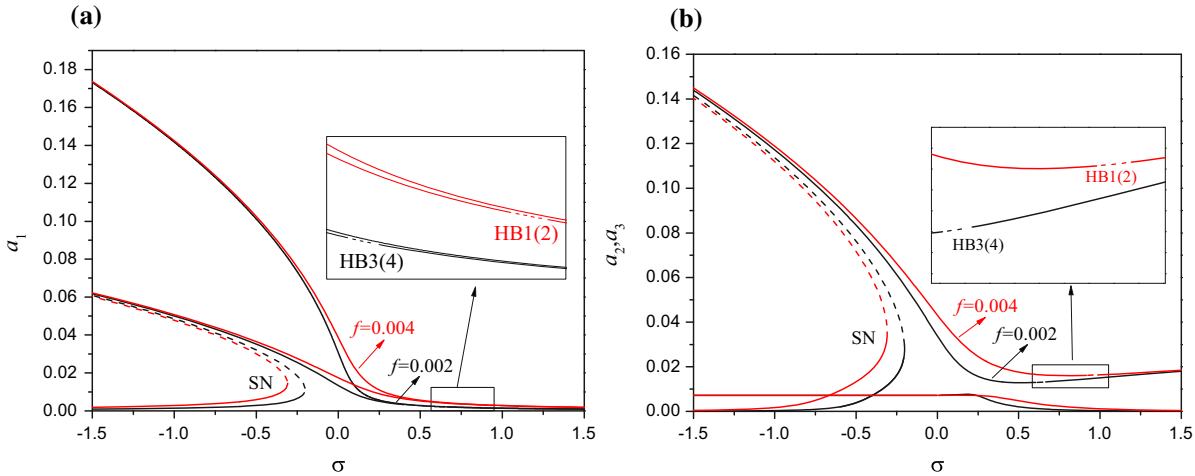

Fig. 4 The frequency–response curves of the arch and cables with different excitation amplitudes when $k_1 = k_2 = k = 1{,}000{,}000$ and $\sigma_1 = \sigma_2 = 6.38 \times 10^{-6}$: **a** for arch, **b** for cables

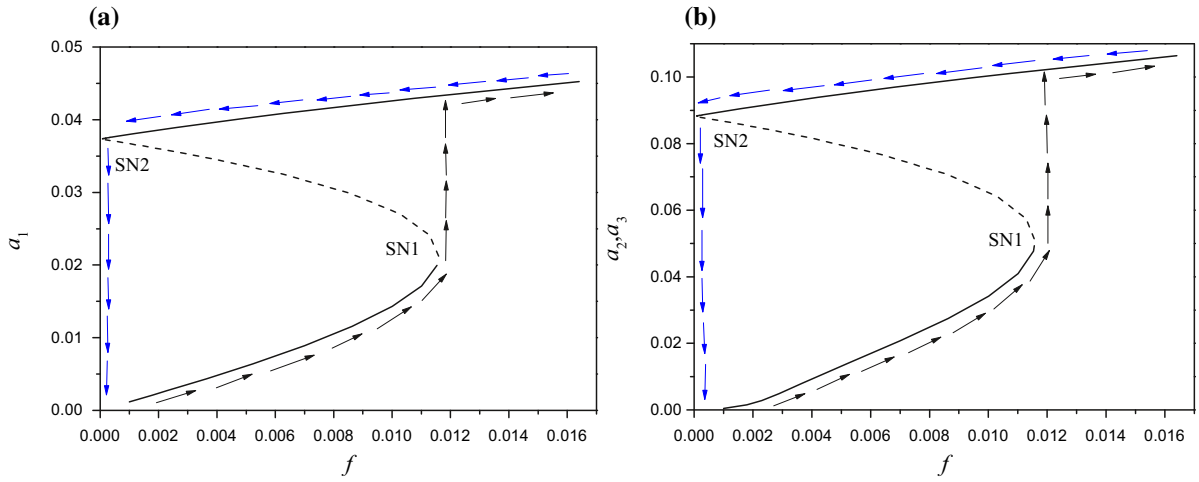

Fig. 5 The force–response curves of the arch and cables with $k_1 = k_2 = k = 1{,}000{,}000$, $\sigma_1 = \sigma_2 = 6.38 \times 10^{-6}$ and $\sigma = -0.6$: **a** for arch, **b** for cables

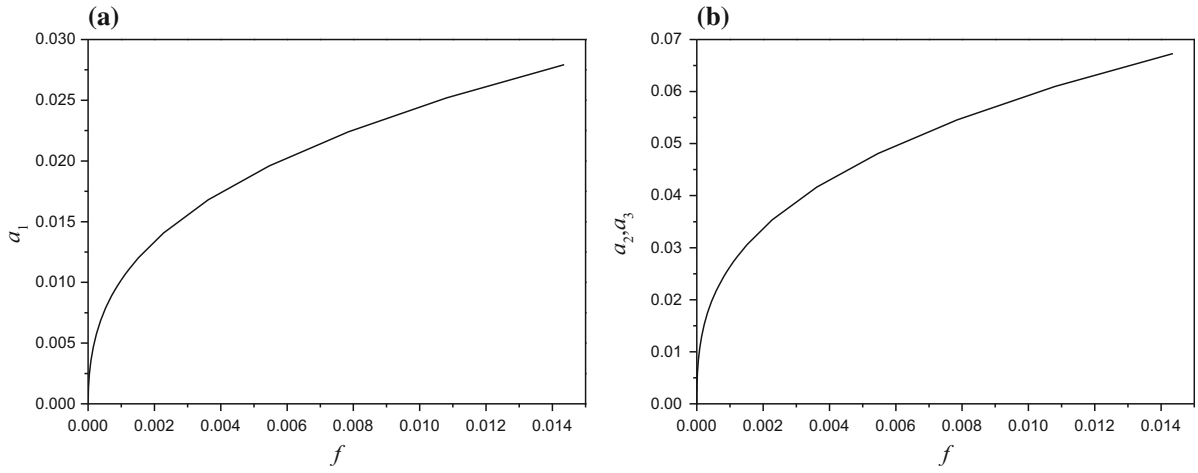

Fig. 6 The force–response curves of the arch and cables with $k_1 = k_2 = k = 1{,}000{,}000$, $\sigma_1 = \sigma_2 = 6.38 \times 10^{-6}$ and $\sigma = 0$: **a** for arch, **b** for cables

the system, the detuning parameter of one cable is changed, which can be achieved by changing the length, initial force, cross-sectional area, Young's modulus and so on. It should be pointed out that the cable whose detuning parameter keeps invariable is named as cable 1, while another cable is named as cable 2. Figures 8, 9 and 10 illustrate the force–response curves of the arch and cables with different internal detuning parameters when $f = 0.001$ and $f = 0.002$. It should be noted that SNs are not marked in these figures, because they are not our focus. Besides, in order to observe the figures clearly, the range of σ is reduced to $[-0.5, 0.5]$.

It can be seen that the difference between the two cables has a great effect on the response of the arch and cable 1, especially when the response amplitude is more than 0.01. However, the difference between the two cables has a slight effect on the response of cable 2 when the response amplitude is less than 0.02 but in general, the effect is small. In a word, the difference between the two cables has a larger effect on the response of the arch and cable 1 than on the cable 2. This shows that changing the internal detuning parameter of one cable has a great influence on the dynamic characteristics of other members, but has little effect on itself. Additionally, with the reduction

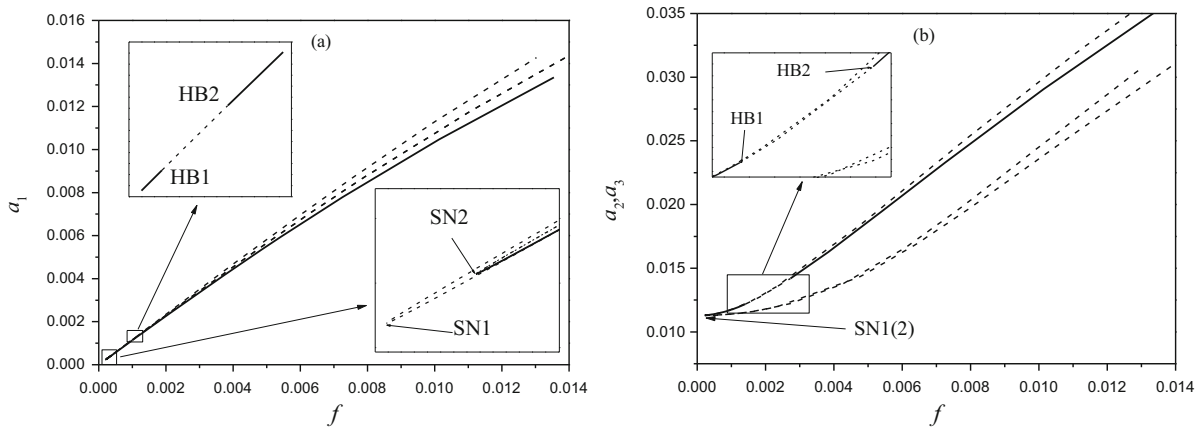

Fig. 7 The force–response curves of the arch and cables with $k_1 = k_2 = k = 1{,}000{,}000$, $\sigma_1 = \sigma_2 = 6.38 \times 10^{-6}$ and $\sigma = 0.6$: **a** for arch, **b** for cables

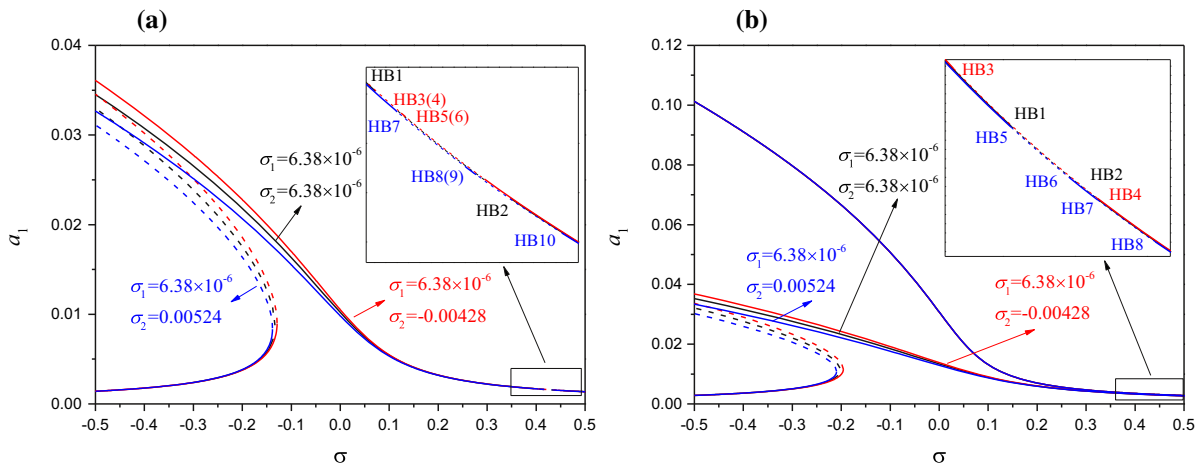

Fig. 8 The frequency-response curves of the arch with different σ_1 and σ_2 when $k_1 = k_2 = k = 1{,}000{,}000$: **a** for $f = 0.001$, **b** for $f = 0.002$

of internal detuning parameter σ_2, the response amplitudes of the arch and cable 1 increase, but it is opposite for the response of cable 2. This may be caused by modal localization and with the increase in internal detuning parameter σ_2, more energy is transferred to cable 1. An interesting phenomenon can be observed in Figs. (b) that the new branch of stable solutions remain unchanged with the variation of σ_2, both for the arch and cables. This may be related to the domain of attraction of the branch, which should attract our attention. It can also be seen that the change of internal detuning parameter σ_2 leads to the occurrence of more HBs, which indicates that the difference between the two cables will result in more complex dynamic behaviors of the system.

Figures 11, 12 and 13 present the force–response curves of the arch and cables with different internal detuning parameters. Different from the frequency–response curves, the difference between cables has an obvious effect on not only the force–response curves of the arch and cable 1, but also those of cable 2 when the external detuning parameter $\sigma = -0.4$ and 0. As seen in Fig. 10a, with the reduction of σ_2, the SNs located at the lower branches gradually shifts outward, which means the range of unstable solutions becomes larger. On the other hand, the SNs located at the upper branches gradually move upward for the arch and

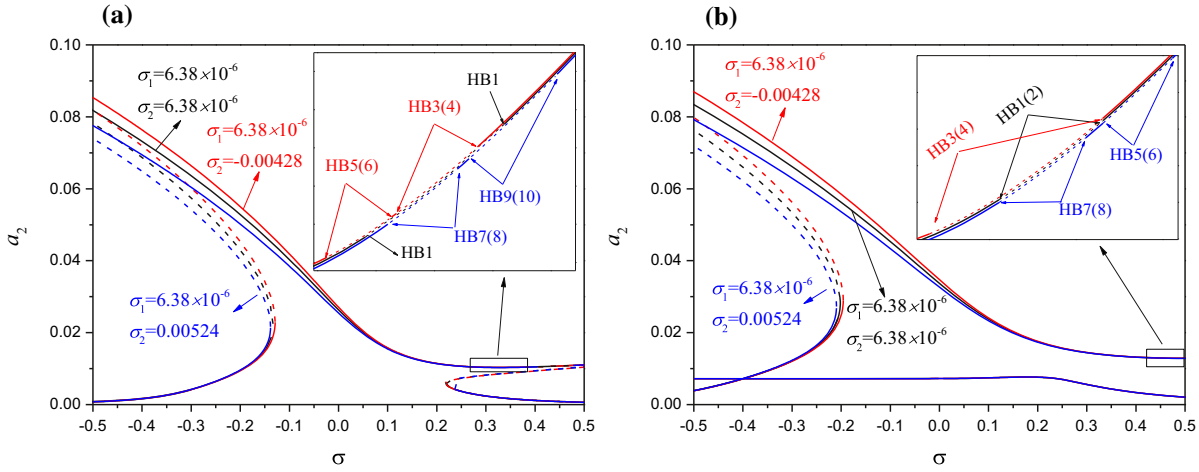

Fig. 9 The frequency-response curves of cable 1 with different σ_1 and σ_2 when $k_1 = k_2 = k = 1{,}000{,}000$: **a** for $f = 0.001$, **b** for $f = 0.002$

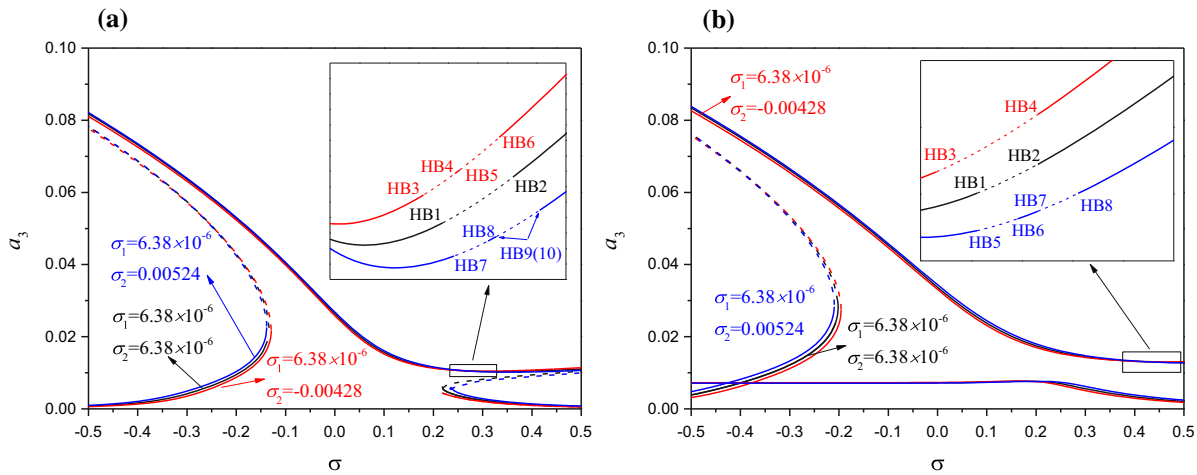

Fig. 10 The frequency-response curves of cable 2 with different σ_1 and σ_2 when $k_1 = k_2 = k = 1{,}000{,}000$: **a** for $f = 0.001$, **b** for $f = 0.002$

cable 1, while for cable 2, these SNs hardly move. What's more, with the reduction of σ_2, the stable solutions of the branches when $\sigma = 0$ and the stable solutions of the upper branches when $\sigma = -0.4$ receive an evident increase for the arch and cable 1. However, it is opposite for cable 2. These phenomena are similar to those in the frequency–response curves. When $\sigma = 0.4$, the difference between cables has a greater influence on the response amplitude of cable 2 itself, while the responses of the arch and cable 1 are almost unaffected, which can also be verified by the lower branches when $\sigma > 0.25$ in Figs. 8b, 9b and 10b.

Next, in order to further explore the effect of the support stiffness on the nonlinear behaviors of the system, we change the support stiffness to $k_1 = k_2 = k = 10{,}000$, which is close to the support stiffness of the bearing in practical engineering. f_0 is set to 0.0643 so that $2\omega_a \approx \omega_b \approx \omega_c$. Figure 14 shows the frequency–response curves of the arch and cables with $k = 10{,}000$. The similar phenomena to those in the case when $k = 1{,}000{,}000$, such as softening characteristic and double-jumping phenomenon, can also be observed and they will not be mentioned, as the new dynamic behaviors are our focus.

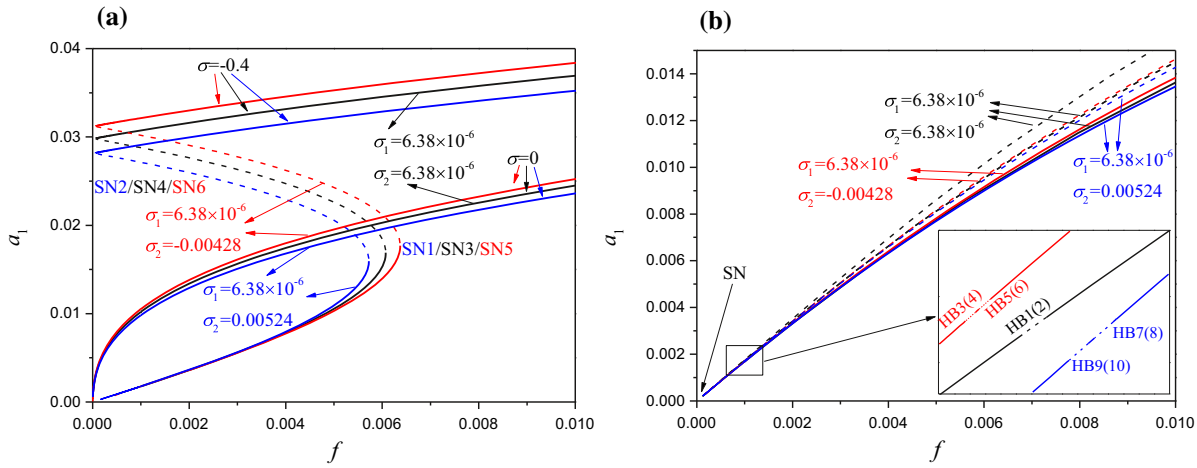

Fig. 11 The force–response curves of the arch with different σ_1 and σ_2 when $k_1 = k_2 = k = 1{,}000{,}000$: **a** for $\sigma = -0.4$ and 0, **b** for $\sigma = 0.4$

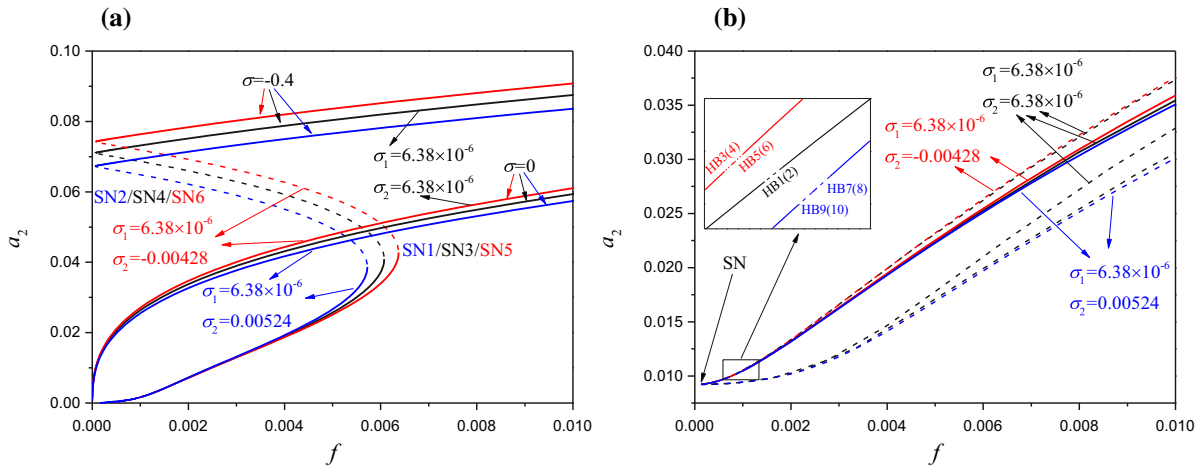

Fig. 12 The force–response curves of cable 1 with different σ_1 and σ_2 when $k_1 = k_2 = k = 1{,}000{,}000$: **a** for $\sigma = -0.4$ and 0, **b** for $\sigma = 0.4$

Comparing Fig. 14 with Fig. 4, an interesting phenomenon can be found. In Fig. 4, when $f = 0.004$ and $\sigma < 0$, there are three branches of stable solutions in total and one of the branch is much larger than the other two. Meanwhile, the double-jumping phenomenon disappears. However, when $k_1 = k_2 = k = 10{,}000$ (see Fig. 14), none of the aforementioned phenomena take place. The reason for these phenomena may be that with the decrease of support stiffness at both ends, the displacement of the support increases, and a part of energy is absorbed by the support, which leads to the decrease in response amplitudes of the arch and cables. However, only when the response amplitudes and energy of the arch and cables reach a certain threshold, new stable branches will appear and double-jumping phenomenon will vanish. In order to verify our conjecture, the excitation amplitude is increased to 0.01 and the corresponding frequency–response curves of the arch and cables are shown in Fig. 15. As can be seen, the new branch of stable solutions appear with no double-jumping phenomenon occurring.

Figure 16 gives the comparison of the frequency–response curves of the arch and cables with different support stiffness when $f = 0.001$. Obviously, the

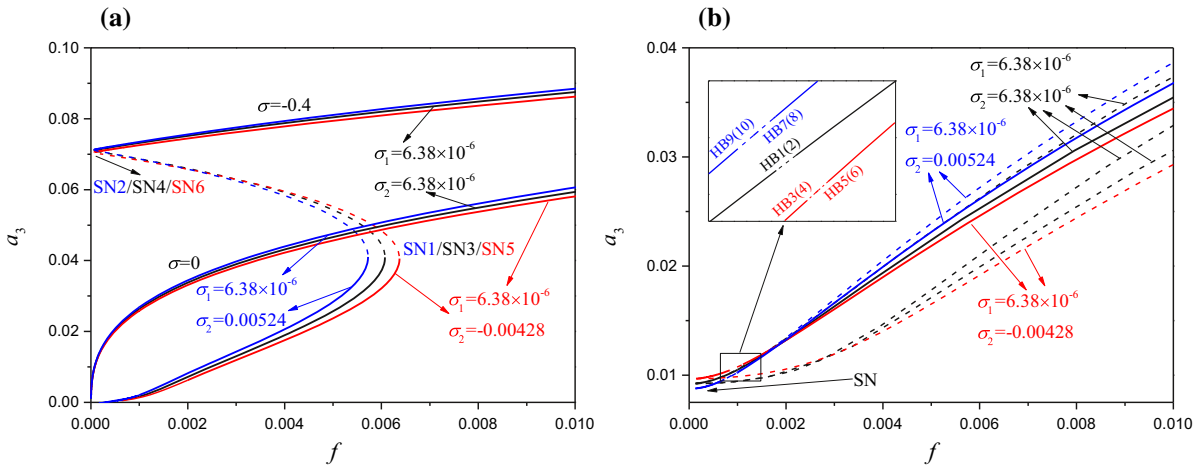

Fig. 13 The force–response curves of cable 2 with different σ_1 and σ_2 when $k_1 = k_2 = k = 1{,}000{,}000$: **a** for $\sigma = -0.4$ and 0, **b** for $\sigma = 0.4$

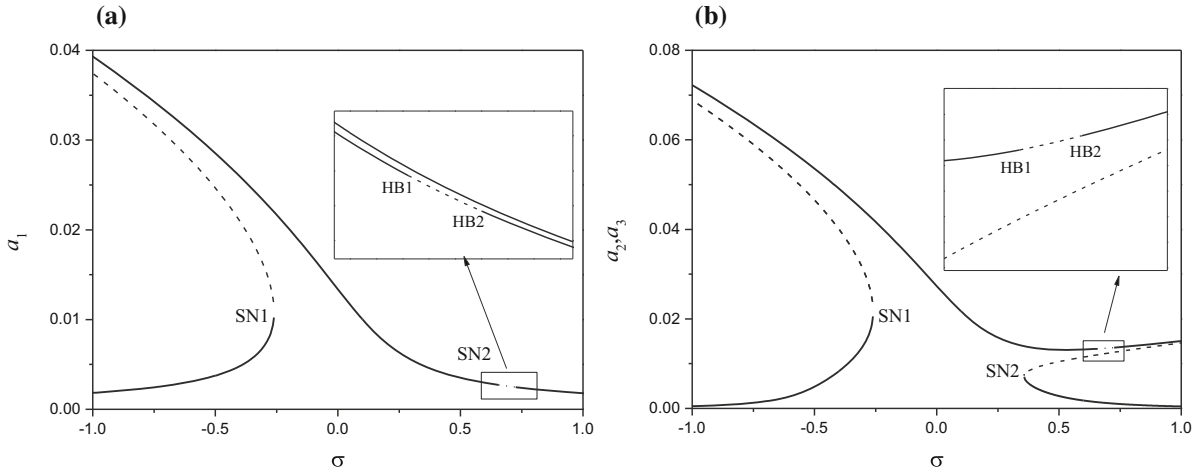

Fig. 14 The frequency–response curves of the arch and cables with $k_1 = k_2 = k = 10{,}000$, $\sigma_1 = \sigma_2 = -5.24 \times 10^{-6}$ and $f = 0.004$: **a** for arch, **b** for cables

response amplitudes of the arch and cables become smaller with the reduction of the support stiffness as a part of energy is absorbed by the support. The maximum amplitude of the arch decreases by 15% and that of cable by 39% due to the reduction of the support stiffness. This means that the reduction of the support stiffness has a larger influence on the response of cables than that of the arch. Due to the fact that the mass of the cable is much smaller than that of the arch, therefore the same energy input can only provide a small vibration of the arch, but can provide a large vibration of the cable. When $k = 10{,}000$, the distance between two SNs is narrowed and unstable solutions caused by HBs move forward.

Figures 17, 18 and 19 are the force–response curves of the arch and cables with different support stiffness. By and large, the response amplitudes of the arch and cables exhibit a consistent trend with the variation of excitation amplitude, namely, the response amplitude of the arch and cables become smaller when $k = 10{,}000$ compared with $k = 1{,}000{,}000$. Similarly to frequency–response curves, the response amplitudes of cables decrease more than those of the arch. With the reduction of the support stiffness, SNs

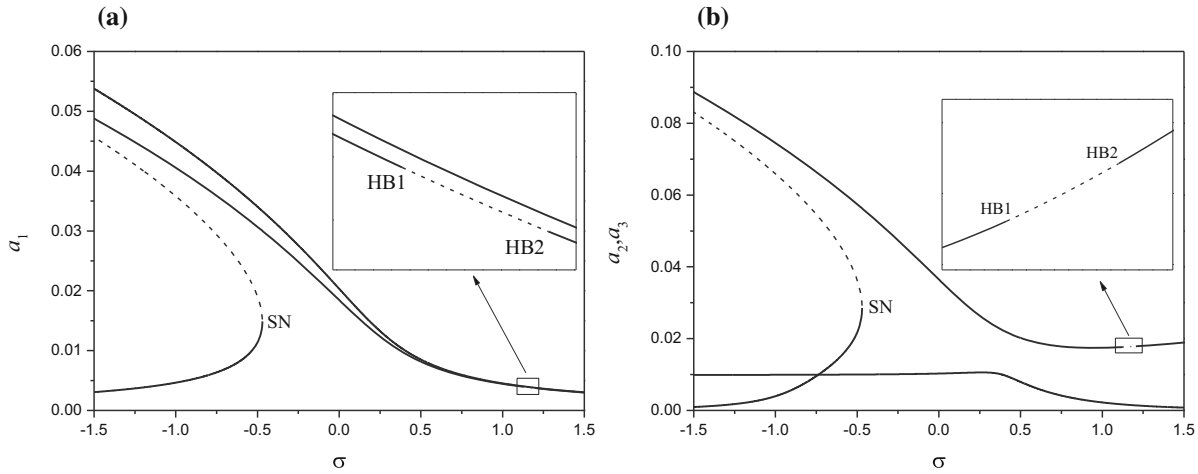

Fig. 15 The frequency–response curves of the arch and cables with $k_1 = k_2 = k = 10{,}000$, $\sigma_1 = \sigma_2 = -5.24 \times 10^{-6}$ and $f = 0.01$: **a** for arch, **b** for cables

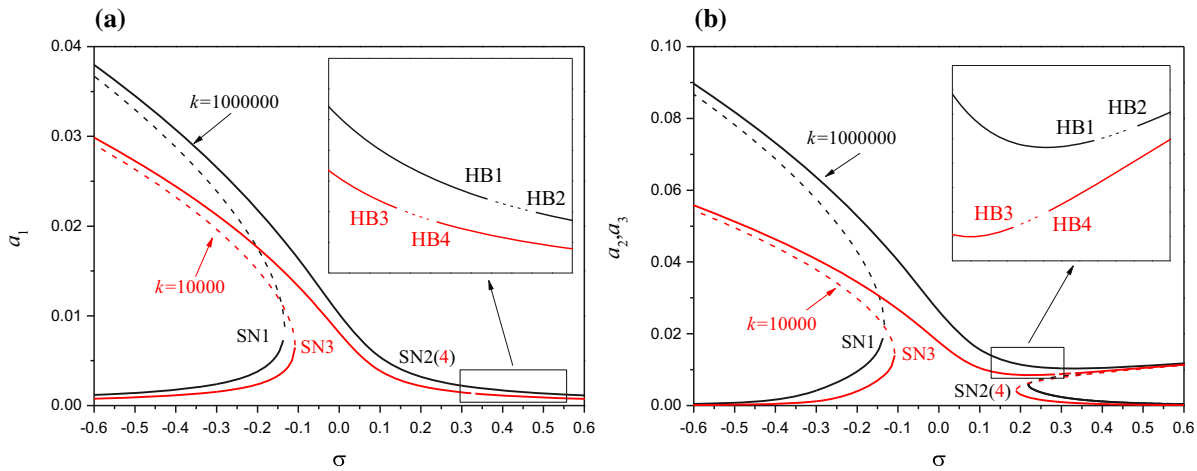

Fig. 16 The frequency–response curves of the arch and cables with different support stiffness when $f = 0.001$ and $\sigma_1 = \sigma_2 = -5.24 \times 10^{-6}$: **a** for arch, **b** for cables

located at the lower branches move outward, which leads to the increase of unstable area between SNs (see Fig. 17). Whereas, when the support stiffness is decreased, HBs move backward (far from the origin, see Fig. 19), which is different from Fig. 16 and may be caused by different energy transfer mechanism.

5 Conclusions

Considering the initial configuration of the beam and vertical elastic supports in cable-stayed bridge, a multi-cable-stayed shallow-arch model is established. Compared with other models, this model is closer to the real cable-stayed bridge in practical engineering. Based on the differential equations governing the planar motion of the arch and cables, the planar eigenvalue problem of the model is solved. In this way, the modal function of the arch is obtained. Then, the 1:2:2 internal resonance among the arch and cables is investigated when the external primary resonance occur. To discretize the differential equations, the Galerkin's method is utilized and a set of ODEs are derived. By using the multiple time scale method, the ODEs are solved and corresponding modulation equations are obtained. The stable solutions of the

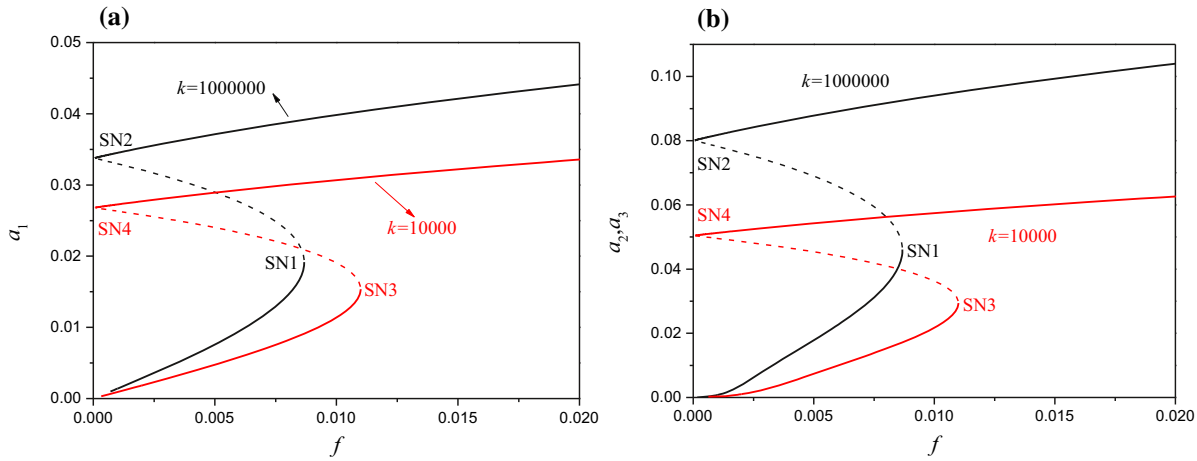

Fig. 17 The force–response curves of the arch and cables with different support stiffness when σ = –0.5 and $\sigma_1 = \sigma_2 = -5.24 \times 10^{-6}$: **a** for arch, **b** for cables

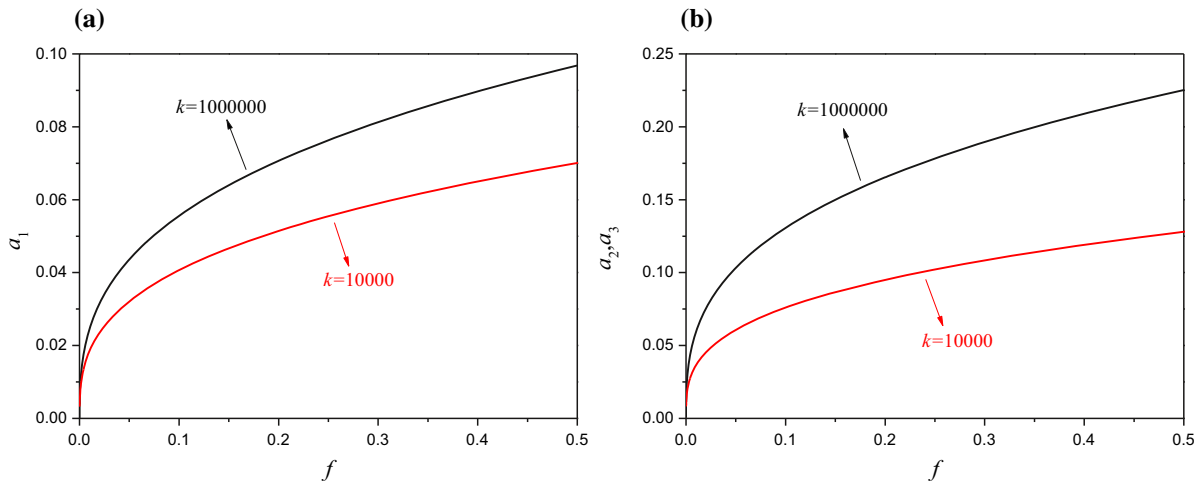

Fig. 18 The force–response curves of the arch and cables with different support stiffness when σ = 0 and $\sigma_1 = \sigma_2 = -5.24 \times 10^{-6}$: **a** for arch, **b** for cables

modulation equations are determined by Newton–Raphson method and continued by pseudo-arclength algorithm. Meanwhile, frequency-/force–response curves are provided to explore the nonlinear behaviors of the system, especially the influence of the support stiffness on the internal resonance of the system. Finally, some interesting conclusions are drawn as follows.

(1) The frequency–response curves of the arch exhibit a softening characteristic, while those of cables exhibit a softening characteristic when $\sigma < 0$ and a hardening characteristic when $\sigma > 0$. Therefore, the double-jumping phenomenon triggered by two SNs is observed in the frequency–response curves of cables.

(2) When the excitation amplitude reaches a certain threshold, the double-jumping phenomenon will vanish and a new branch of stable solutions appear and its value is obviously larger than other branches. The support stiffness is one of the key factors that affect the value of threshold.

(3) Changing the internal detuning parameter of one cable has a great influence on the frequency–response curves of other members, but has little

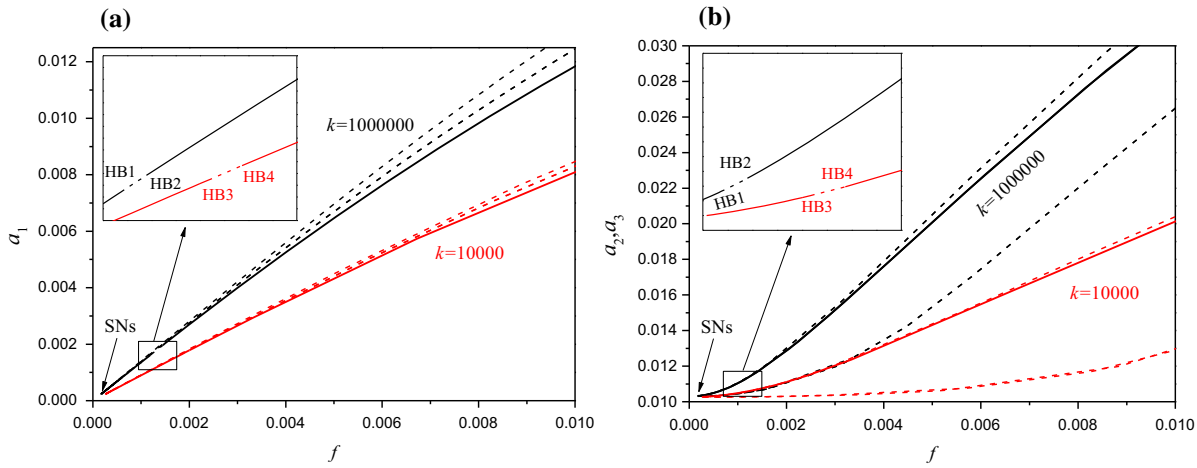

Fig. 19 The force–response curves of the arch and cables with different support stiffness when $\sigma = 0.5$ and $\sigma_1 = \sigma_2 = -5.24 \times 10^{-6}$: **a** for arch, **b** for cables

effect on itself. With the reduction of internal detuning parameter, the frequency–response amplitudes of the cable whose internal detuning parameter changes are decreased, but it is opposite for the response of the arch and another cable. Moreover, the difference between cables will lead to more complicated dynamic behaviors of the system.

(4) With the reduction of the support stiffness, the response amplitudes of the arch and cables will become smaller as the supports absorb a part of energy. The support stiffness has a greater influence on the response curves of cables than on those of the arch. Due to the existence of elastic supports, the threshold of the excitation amplitude making the double-jumping phenomenon disappear becomes larger.

Acknowledgements The authors wish to acknowledge the support of the National Natural Science Foundation of China (11972151 and 11872176).

Declarations

Conflict of interest The authors declare that they have no conflict of interests.

Appendix A

This paper considers a model with two cables the model is assumed to be symmetrical. Since the parameters of the two cables are identical, the subscripts 'i' and 'j' of some variables are dropped in the following expressions. For the sake of convenience, the following variables are introduced.

$$W_1 = \frac{\beta_a f_0^2 \eta_a \pi^2}{\beta_a^2 + \pi^2}, W_2 = \frac{\beta_a f_0^2 \eta_a \pi^2}{\beta_a^2 - \pi^2}, \delta_{11} = \cos(\beta_a s_1),$$
$$\delta_{12} = \sin(\beta_a s_1), \delta_{21} = \cos(\beta_a s_2), \delta_{22} = \sin(\beta_a s_2),$$
$$\delta_{31} = \cos(\pi s_1), \delta_{32} = \sin(\pi s_1),$$
$$\delta_{41} = \cos(\pi s_2), \delta_{42} = \sin(\pi s_2),$$
$$\delta_{51} = \cosh(\beta_a s_1), \delta_{52} = \sinh(\beta_a s_1),$$
$$\delta_{61} = \cosh(\beta_a s_2), \delta_{62} = \sinh(\beta_a s_2)$$

In this way, the elements of the matrix [**T**] in Eq. (35) can be expressed as.

$$
\begin{aligned}
t_{1,1} &= \eta_{11}, t_{1,2} = 1 + \eta_{12}, t_{2,3} = \eta_{21}, t_{2,4} = 1 + \eta_{22},\\
t_{3,1} &= \eta_{11} + \sin\beta_c, t_{3,2} = \eta_{12} + \cos\beta_c, t_{3,5}\\
&= -\gamma_{c1}\delta_{11}\cos\theta,\\
t_{3,6} &= -\gamma_{c1}\delta_{12}\cos\theta, t_{3,7} = -\gamma_{c1}\delta_{51}\cos\theta, t_{3,8}\\
&= -\gamma_{c1}\delta_{52}\cos\theta, t_{3,9}\\
t_{4,3} &= \eta_{21} + \sin\beta_c,\\
t_{4,4} &= \eta_{22} + \cos\beta_c,\\
t_{4,10} &= -\gamma_{c2}\delta_{21}\cos\theta,\\
t_{4,11} &= -\gamma_{c2}\delta_{22}\cos\theta, t_{4,12} = -\gamma_{c2}\delta_{61}\cos\theta, t_{4,13}\\
&= -\gamma_{c2}\delta_{62}\cos\theta,\\
t_{4,14} &= -\gamma_{c2}\delta_{42}\cos\theta, t_{5,5}\\
&= k_1 + W_2(\beta_a - \beta_a\delta_{11}\delta_{31} - \pi\delta_{12}\delta_{32}),\\
t_{5,6} &= -\beta_a^3 - W_2(\beta_a\delta_{31}\delta_{12} - \pi\delta_{11}\delta_{32}),\\
t_{5,7} &= k_1 + W_1(\beta_a - \beta_a\delta_{31}\delta_{51} - \pi\delta_{32}\delta_{52}),\\
t_{5,8} &= \beta_a^3 - W_1(\pi\delta_{32}\delta_{51} + \beta_a\delta_{31}\delta_{52}),\\
t_{5,9} &= -\pi^3 - \frac{1}{2}f_0^2\eta_a\pi^3 s_1 - \frac{1}{4}f_0^2\eta_a\pi^2\sin(2\pi s_1),\\
t_{5,10} &= W_2(\beta_a\delta_{11}\delta_{31} - \beta_a\delta_{21}\delta_{41} + \pi\delta_{12}\delta_{32} - \pi\delta_{22}\delta_{42}), t_{5,11}\\
&= W_2(\beta_a\delta_{12}\delta_{31} - \pi\delta_{11}\delta_{32} - \beta_a\delta_{22}\delta_{41} + \pi\delta_{21}\delta_{42}),\\
t_{5,12} &= W_1(\beta_a\delta_{51}\delta_{31} - \beta_a\delta_{61}\delta_{41} + \pi\delta_{52}\delta_{32} - \pi\delta_{62}\delta_{42}),\\
t_{5,13} &= W_1(\pi\delta_{51}\delta_{32} - \pi\delta_{61}\delta_{42} + \beta_a\delta_{52}\delta_{31} - \beta_a\delta_{62}\delta_{41}),\\
t_{5,14} &= \frac{1}{2}f_0^2\eta_a\pi^3 s_1 - \frac{1}{2}f_0^2\eta_a\pi^3 s_2 + \frac{1}{4}f_0^2\eta_a\pi^2\sin(2\pi s_1)\\
&\quad - \frac{1}{4}f_0^2\eta_a\pi^2\sin(2\pi s_2),\\
t_{5,15} &= W_2(\beta_a\cos\beta_a + \beta_a\delta_{21}\delta_{41} + \pi\delta_{22}\delta_{42}),\\
t_{5,16} &= W_2(\beta_a\sin\beta_a + \beta_a\delta_{22}\delta_{41} - \pi\delta_{21}\delta_{42}),\\
t_{5,17} &= W_1(\beta_a\cosh\beta_a + \beta_a\delta_{61}\delta_{41} + \pi\delta_{62}\delta_{42}),\\
t_{5,18} &= W_1(\pi\delta_{61}\delta_{42} + \beta_a\sinh\beta_a + \delta_{62}\delta_{41}),\\
t_{5,19} &= -\frac{1}{2}f_0^2\eta_a\pi^3 + \frac{1}{2}f_0^2\eta_a\pi^3 s_2 + \frac{1}{4}f_0^2\eta_a\pi^2\sin(2\pi s_2),\\
t_{6,5} &= k_1 - t_{5,5}, t_{6,6} = -\beta_a^3 - t_{5,6,6,7}\\
t_{6,9} &= -\pi^3 - t_{5,9}, t_{6,10} = -t_{5,10},\\
t_{6,11} &= -t_{5,11}, t_{6,12} = -t_{5,12}, t_{6,13} = -t_{5,13}, t_{6,14} = -t_{5,14},\\
t_{6,15} &= \beta_a^3\sin\beta_a - k_2\cos\beta_a - t_{5,15},\\
t_{6,16} &= -\beta_a^3\cos\beta_a - k_2\sin\beta_a - t_{5,16},\\
t_{6,17} &= \beta_a^3\sinh\beta_a - k_2\cosh\beta_a - t_{5,17},\\
t_{6,18} &= \beta_a^3\cosh\beta_a - k_2\sinh\beta_a - t_{5,18}, t_{6,19} = \pi^3 - t_{5,19},\\
t_{7,5} &= -1, t_{7,7} = 1, t_{8,15} = -\cos\beta_a,\\
t_{8,16} &= -\sin\beta_a, t_{8,17} = \cosh\beta_a, t_{8,18} = \sinh\beta_a, t_{9,5} = \delta_{11},\\
t_{9,6} &= \delta_{12}, t_{9,7} = \delta_{51}, t_{9,8} = \delta_{52},\\
t_{9,9} &= \delta_{32}, t_{9,10} = -\delta_{11}, t_{9,11} = -\delta_{12},\\
t_{9,12} &= -\delta_{51}, t_{9,13} = -\delta_{52},\\
t_{9,14} &= -\delta_{32}, t_{10,5} = -\beta_a\delta_{12},\\
t_{10,6} &= \beta_a\delta_{11}, t_{10,7} = \beta_a\delta_{52}, t_{10,8} = \beta_a\delta_{51},\\
t_{10,9} &= \pi\delta_{31}, t_{10,10} = \beta_a\delta_{12}, t_{10,11} = -\beta_a\delta_{11},\\
t_{10,12} &= -\beta_a\delta_{52}, t_{10,13} = -\beta_a\delta_{51}, t_{10,14} = -\pi\delta_{31},\\
t_{11,5} &= -\beta_a^2\delta_{11}, t_{11,6} = -\beta_a^2\delta_{12}, t_{11,7} = \beta_a^2\delta_{51},\\
t_{11,8} &= \beta_a^2\delta_{52}, t_{11,9} = -\pi^2\delta_{32}, t_{11,10} = \beta_a^2\delta_{11},\\
t_{11,11} &= \beta_a^2\delta_{12}, t_{11,12} = -\beta_a^2\delta_{51},\\
t_{11,13} &= -\beta_a^2\delta_{52}, t_{11,14} = \pi^2\delta_{32}, t_{12,10} = \delta_{21},\\
t_{12,11} &= \delta_{22}, t_{12,12} = \delta_{61}, t_{12,13} = \delta_{62}, t_{12,14} = \delta_{42},\\
t_{12,15} &= -\delta_{21}, t_{12,16} = -\delta_{22}, t_{12,17} = -\delta_{61},\\
t_{12,18} &= -\delta_{62}, t_{12,19} = -\delta_{42}, t_{13,10} = -\beta_a\delta_{22},\\
t_{13,11} &= \beta_a\delta_{21}, t_{13,12} = \beta_a\delta_{62},\\
t_{13,13} &= \beta_a\delta_{61}, t_{13,14} = \pi\delta_{41}, t_{13,15} = \beta_a\delta_{22},\\
t_{13,16} &= -\beta_a\delta_{21}, t_{13,17} = -\beta_a\delta_{62}, t_{13,18} = -\beta_a\delta_{61},\\
t_{13,19} &= -\pi\delta_{41}, t_{14,10} = -\beta_a^2\delta_{21}, t_{14,11} = -\beta_a^2\delta_{22},\\
t_{14,12} &= \beta_a^2\delta_{61}, t_{14,13} = \beta_a^2\delta_{62}, t_{14,14} = -\pi^2\delta_{42},\\
t_{14,15} &= \beta_a^2\delta_{21}, t_{14,16} = \beta_a^2\delta_{22}, t_{14,17} = -\beta_a^2\delta_{61},\\
t_{14,18} &= -\beta_a^2\delta_{62}, t_{15,1} = -\frac{\beta_c\cos\beta_c\cos\theta}{\mu_c}\\
&\quad + (4d\cos\theta - \sin\theta)(\frac{8d}{\beta_c} - \frac{8d\cos\beta_c}{\beta_c}\\
&\quad - 4d\sin\beta_c + \eta_{11}\tan\theta + \sin\beta_c\tan\theta),\\
t_{14,19} &= \pi^2\delta_{42}, t_{15,2}\\
&= \frac{\beta_c\sin\beta_c\cos\theta}{\mu_c} + (4d\cos\theta - \sin\theta)\\
&\quad (-4d - 4d\cos\beta_c + \frac{8d\sin\beta_c}{\beta_c}\\
&\quad + \eta_{12}\tan\theta + \cos\beta_c\tan\theta),\\
t_{15,5} &= \beta_a^3\chi\delta_{12}, t_{15,6} = -\beta_a^3\chi\delta_{11}, t_{15,7} = \beta_a^3\chi\delta_{52},\\
t_{15,8} &= \beta_a^3\chi\delta_{51}, t_{15,9} = -\pi^3\chi\delta_{31},\\
t_{15,10} &= -\beta_a^3\chi\delta_{12}, t_{15,11} = \beta_a^3\chi\delta_{11},\\
t_{15,12} &= -\beta_a^3\chi\delta_{52}, t_{15,13} = -\beta_a^3\chi\delta_{51}, t_{15,14} = \pi^3\chi\delta_{31},
\end{aligned}
$$

$$
\begin{aligned}
t_{16,3} &= -\frac{\beta_c \cos\beta_c \cos\theta}{\lambda_c} + (4d\cos\theta - \sin\theta) \\
&\quad \times \left(\frac{8d}{\beta_c} - \frac{8d\cos\beta_c}{\beta_c} - 4d\sin\beta_c \right. \\
&\quad \left. + \eta_{21}\tan\theta + \sin\beta_c \tan\theta\right), \\
t_{16,4} &= \frac{\beta_c \sin\beta_c \cos\theta}{\mu_c} + (4d\cos\theta - \sin\theta) \\
&\quad \times \left(-4d - 4d\cos\beta_c + \frac{8d_c \sin\beta_c}{\beta_c} \right. \\
&\quad \left. + \eta_{22}\tan\theta + \cos\beta_c \tan\theta\right), \\
t_{16,10} &= \beta_a^3 \chi\delta_{22}, t_{16,11} = -\beta_a^3\chi\delta_{21}, t_{16,12} = \beta_a^3\chi\delta_{62}, \\
t_{16,13} &= \beta_a^3\chi\delta_{61}, t_{16,14} = -\pi^3\chi\delta_{41}, \\
t_{16,15} &= -\beta_a^3\chi\delta_{22}, t_{16,16} = \beta_a^3\chi\delta_{21}, \\
t_{16,17} &= -\beta_a^3\chi\delta_{62}, t_{16,18} = -\beta_a^3\chi\delta_{61}, \\
t_{16,19} &= \pi^3\chi\delta_{41}, t_{17,5} = t_{18,5} = t_{19,5} \\
&= W_2\pi(-\beta_a + \beta_a\delta_{31}\delta_{11} + \pi\delta_{32}\delta_{12}), \\
t_{17,6} &= t_{18,6} = t_{19,6} = W_2\pi(\beta_a\delta_{31}\delta_{12} - \pi\delta_{32}\delta_{11}), \\
t_{17,7} &= t_{18,7} = t_{19,7} = W_1\pi(-\beta_a + \beta_a\delta_{31}\delta_{51} + \pi\delta_{32}\delta_{52}), \\
t_{17,8} &= t_{18,8} = t_{19,8} = W_1\pi(\pi\delta_{32}\delta_{51} + \beta_a\delta_{31}\delta_{52}), \\
t_{17,9} &= -4\beta_a^4 + 2\pi^4(2 + f_0^2 s_1\eta_a) + f_0^2\pi^3\eta_a \sin 2\pi s_1, \\
t_{19,9} &= t_{18,9} = f_0^2\pi^3\eta_a(2\pi s_1 + \sin 2\pi s_1), \\
t_{17,10} &= t_{18,10} = t_{19,10} \\
&= W_2\pi(\beta_a\delta_{41}\delta_{21} - \beta_a\delta_{31}\delta_{11} - \pi\delta_{32}\delta_{12} + \pi\delta_{42}\delta_{22}), \\
t_{17,11} &= t_{18,11} = t_{19,11} \\
&= W_2\pi(\pi\delta_{11}\delta_{32} - \beta_a\delta_{31}\delta_{12} + \beta_a\delta_{41}\delta_{22} - \pi\delta_{21}\delta_{42}), \\
t_{17,12} &= t_{18,12} = t_{19,12} \\
&= W_1\pi(\beta_a\delta_{41}\delta_{61} - \beta_a\delta_{31}\delta_{51} - \pi\delta_{32}\delta_{52} + \pi\delta_{42}\delta_{62}), \\
t_{17,13} &= t_{18,13} = t_{19,13} \\
&= W_1\pi(-\pi\delta_{51}\delta_{32} + \pi\delta_{61}\delta_{42} - \beta_a\delta_{31}\delta_{52} + \beta_a\delta_{41}\delta_{62}), \\
t_{19,14} &= t_{17,14} = f_0^2\pi^3\eta_a(2\pi(-s_1 + s_2) - \sin 2\pi s_1 + \sin 2\pi s_2), \\
t_{18,14} &= 4\pi^4 - 4\beta_a^4 \\
&\quad + f_0^2\pi^3\eta_a(2\pi(-s_1 + s_2) - \sin 2\pi s_1 + \sin 2\pi s_2), \\
t_{17,15} &= t_{18,15} = t_{19,15} \\
&= -W_2\pi(\beta_a\cos\beta_a + \beta_a\delta_{41}\delta_{21} + \pi\delta_{42}\delta_{22}), \\
t_{17,16} &= t_{18,16} = t_{19,16} \\
&= -W_2\pi(\beta_a\sin\beta_a + \beta_a\delta_{41}\delta_{22} - \pi\delta_{21}\delta_{42}), \\
t_{17,17} &= t_{18,17} = t_{19,17} \\
&= -W_1\pi(\beta_a\cosh\beta_a + \beta_a\delta_{41}\delta_{61} + \pi\delta_{62}\delta_{42}), \\
t_{17,18} &= t_{18,18} = t_{19,18} \\
&= -W_1\pi(\pi\delta_{61}\delta_{42} + \beta_a\sinh\beta_a + \beta_a\delta_{41}\delta_{62}), \\
t_{18,19} &= t_{17,19} = -f_0^2\pi^3\eta_a(2\pi(-1 + s_2) + \sin 2\pi s_2), \\
t_{19,19} &= -(4\beta_a^4 + 2\pi^4(-2 + f_0^2(-1 + s_2)\eta_a + f_0^2\pi^3\eta_a \sin 2\pi s_2).
\end{aligned}
$$

Appendix B

First, the following integrals are introduced.

$$
\begin{aligned}
d_{mm} &= \int_0^1 y_m'\varphi_m' dx_m, d_{33} = \int_0^1 y_0'(x)\phi_a'(x)dx, \\
d_{0m} &= \int_0^1 \varphi_m' dx_m, d_{m0} = \int_0^1 y_m' dx_m, \\
f_{mm} &= \int_0^1 y_m''\varphi_m dx_m, , \\
h_{mm} &= \int_0^1 \varphi_m\varphi_m'' dx_m, l_{mm} = \int_0^1 \varphi_m'\varphi_m' dx_m, \\
s_{mm} &= \int_0^1 x_m\varphi_m dx_m, r_{33} = \int_0^1 \phi_a''''\phi_a dx, \\
\Gamma_{mm} &= 1\Big/\int_0^1 \varphi_m\varphi_m dx_m, \quad (m = 0, 1, 2, 3).,
\end{aligned}
$$

where $m = 0$ represents there is no corresponding term, φ_m and y_m are the modal functions and initial configurations of the arch and cables, respectively, and $\varphi_3 = \phi_a$, $y_3 = y_0$. Then, Galerkin's integral coefficients in Eqs. (40) and (41) can be expressed as

$$
\begin{aligned}
b_{11} &= \omega_a^2 = \Gamma_{33}(r_{33} - \eta d_{33} f_{33})/\beta_a^4 \\
&\quad - \frac{1}{2}\Gamma_{33}\sum_{j=1}^{2} d_{j0} K_j \phi^2(s_j)\sin 2\theta_j \\
&\quad + \Gamma_{33}\sum_{j=1}^{2}\gamma_{cj} K_j \phi^2(s_j)\sin^2\theta_j, \\
b_{12} &= -\frac{1}{2}\eta\Gamma_{33} d_{03} f_{33}/\beta_a^4 - \eta\Gamma_{33} d_{33} h_{33}/\beta_a^4 \\
&\quad - \frac{1}{2}\Gamma_{33}\sum_{j=1}^{2} K_j \phi^3(s_j)\cos^2\theta_j \sin\theta_j, \\
b_{13} &= -\frac{1}{2}\eta\Gamma_{33} d_{03} h_{33}/\beta_a^4, b_{14} \\
&= -\Gamma_{33} K_1 d_{11}\phi_a(s_1)\sin\theta_1, b_{15} \\
&= -\frac{1}{2}\Gamma_{33} K_1 \phi^2(s_1)\sin 2\theta_1 d_{01}, \\
b_{16} &= -\Gamma_{33} K_2 \phi_a(s_2)\sin\theta_2 d_{22}, b_{17} \\
&= -\frac{1}{2}\Gamma_{33} K_2 \phi^2(s_2)\sin 2\theta_2 d_{02}, b_{18} \\
&= -\frac{1}{2}\Gamma_{33} K_1 \phi_a(s_1)\sin\theta_1, \\
b_{19} &= -\frac{1}{2}\Gamma_{33} K_2 \phi_a(s_2)\phi_a(s_2)\sin\theta_2 l_{22}, b_{110} \\
&= -\Gamma_{33} f h_{30}, b_{(j+1)1} \\
&= \Gamma_{(j+1)(j+1)}\mu_{cj}\cos\theta_j \phi_a(s_j) s_{jj}, \\
b_{(j+1)2} &= \Gamma_{(j+1)(j+1)}\cos\theta_j \phi_a(s_j) s_{jj}, \\
b_{(j+1)3} &= -\Gamma_{(j+1)(j+1)}\lambda_{cj}\cos\theta_j \phi_a(s_j) d_{j0} f_{jj}/\beta_{cj}^2 \\
&\quad + \Gamma_{(j+1)(j+1)}\lambda_{cj}\gamma_{cj}\sin\theta_j \phi_a(s_j) f_{jj}, \\
b_{(j+1)4} &= \omega_b^2 = -\Gamma_{(j+1)(j+1)}\lambda_{cj} d_{jj} f_{jj}/\beta_{cj}^2 \\
&\quad - \Gamma_{(j+1)(j+1)} h_{jj}/\beta_{cj}^2, b_{(j+1)5} \\
&= -\frac{1}{2}\Gamma_{(j+1)(j+1)}\lambda_{cj}\cos^2\theta_j \phi_a^2(s_j) f_{jj}/\beta_{cj}^2, \\
b_{(j+1)6} &= -\Gamma_{(j+1)(j+1)}\lambda_{cj}\cos\theta_j \phi_a(s_j)(d_{0j} f_{jj} \\
&\quad + d_{j0} h_{jj})/\beta_{cj}^2 + \Gamma_{(j+1)(j+1)}\gamma_{cj}\lambda_{cj}\sin\theta_j \phi_a(s_j) h_{jj}/\beta_{cj}^2, \\
b_{(j+1)7} &= -\frac{1}{2}\Gamma_{(j+1)(j+1)}\lambda_{cj} l_{jj} f_{jj}/\beta_{cj}^2 \\
&\quad - \Gamma_{(j+1)(j+1)}\lambda_{cj} d_{jj} h_{jj}/\beta_{cj}^2, b_{(j+1)8} \\
&= -\frac{1}{2}\Gamma_{(j+1)(j+1)}\lambda_{cj}\cos^2\theta_j \phi_a^2(s_j) h_{jj}/\beta_{cj}^2, \\
b_{(j+1)9} &= -\Gamma_{(j+1)(j+1)}\lambda_{cj}\cos\theta_j \phi_a(s_j) d_{0j} h_{jj}/\beta_{cj}^2, b_{(j+1)10} \\
&= -\frac{1}{2}\Gamma_{(j+1)(j+1)}\lambda_{cj} l_{jj} h_{jj}/\beta_{cj}^2 \quad (j = 1, 2).
\end{aligned}
$$

Appendix C

The coefficients in Eqs. (50)–(52) are defined as

$$
\begin{aligned}
\Gamma_a^1 &= -3b_{13} + \frac{2b_{15}b_{25}}{\omega_b^2} - \frac{b_{15}b_{25}}{4\omega_a^2 - \omega_b^2} + \frac{2b_{17}b_{35}}{\omega_c^2} \\
&\quad - \frac{b_{17}b_{35}}{4\omega_a^2 - \omega_c^2} + \frac{10b_{12}^2}{3\omega_a^2}, \Gamma_a^2 = -\frac{b_{14}b_{23}}{\omega_a^2 - \omega_b^2} - \frac{b_{16}b_{33}}{\omega_a^2 - \omega_c^2}, \\
\Gamma_a^3 &= \frac{2b_{15}b_{27}}{\omega_b^2} - \frac{2b_{18}b_{26}}{\omega_a^2 - 2\omega_a\omega_b} - \frac{2b_{18}b_{26}}{\omega_a^2 + 2\omega_a\omega_b} \\
&\quad + \frac{2b_{12}b_{18}}{\omega_a^2} + \frac{b_{15}^2}{2\omega_a\omega_b - \omega_b^2} - \frac{b_{15}^2}{2\omega_a\omega_b + \omega_b^2}, \\
\Gamma_a^4 &= \frac{2b_{17}b_{37}}{\omega_c^2} - \frac{2b_{19}b_{36}}{\omega_a^2 - 2\omega_a\omega_c} + \frac{2b_{19}b_{36}}{\omega_a^2 + 2\omega_a\omega_c} \\
&\quad + \frac{4b_{12}b_{19}}{\omega_a^2} + \frac{b_{17}^2}{2\omega_a\omega_c - \omega_c^2} - \frac{b_{17}^2}{2\omega_a\omega_c + \omega_c^2}, \\
\Gamma_a^5 &= -\frac{b_{14}b_{26}}{\omega_a^2 - 2\omega_a\omega_b} - \frac{2b_{18}b_{23}}{\omega_a^2 - \omega_b^2} - \frac{2b_{12}b_{14}}{-\omega_a^2 + \omega_b^2}, \\
\Gamma_a^6 &= -\frac{b_{16}b_{36}}{\omega_a^2 - 2\omega_a\omega_c} - \frac{2b_{19}b_{33}}{\omega_a^2 - \omega_c^2} - \frac{2b_{12}b_{16}}{-\omega_a^2 + \omega_c^2}, \\
\Gamma_a^7 &= -\frac{b_{15}b_{17}}{2\omega_a\omega_c + \omega_c^2} + \frac{b_{15}b_{17}}{2\omega_a\omega_b - \omega_b^2}, \\
\Gamma_a^8 &= \frac{b_{15}b_{17}}{2\omega_a\omega_c - \omega_c^2} - \frac{b_{15}b_{17}}{2\omega_a\omega_b + \omega_b^2}, \\
\Gamma_b^1 &= -2b_{28} - \frac{b_{26}^2}{\omega_a^2 - 2\omega_a\omega_b} - \frac{b_{26}^2}{\omega_a^2 + 2\omega_a\omega_b} + \frac{4b_{25}b_{27}}{\omega_b^2} \\
&\quad + \frac{2b_{15}b_{25}}{2\omega_a\omega_b - \omega_b^2} - \frac{2b_{15}b_{25}}{2\omega_a\omega_b + \omega_b^2} + \frac{2b_{12}b_{26}}{\omega_a^2}, \\
\Gamma_b^2 &= -3b_{210} + \frac{10b_{27}^2}{3\omega_b^2} + \frac{2b_{18}b_{26}}{\omega_a^2} + \frac{b_{18}b_{26}}{\omega_a^2 - 4\omega_b^2}, \\
\Gamma_b^3 &= -\frac{b_{14}b_{23}}{-\omega_a^2 + \omega_b^2}, \Gamma_b^4 = \frac{2b_{19}b_{26}}{\omega_a^2}, \\
\Gamma_b^5 &= -\frac{b_{23}b_{26}}{\omega_a^2 - \omega_b^2} - \frac{b_{12}b_{23}}{3\omega_a^2}, \\
\Gamma_b^6 &= -\frac{b_{16}b_{23}}{-\omega_a^2 + \omega_c^2}, \Gamma_b^7 = \frac{2b_{17}b_{25}}{2\omega_a\omega_c - \omega_c^2} - \frac{2b_{17}b_{25}}{2\omega_a\omega_c + \omega_c^2}, \\
\Gamma_b^8 &= \frac{b_{19}b_{26}}{\omega_a^2 - 4\omega_c^2}, \\
\Gamma_c^1 &= -2b_{38} - \frac{b_{36}^2}{\omega_a^2 - 2\omega_a\omega_c} - \frac{b_{36}^2}{\omega_a^2 + 2\omega_a\omega_c} + \frac{4b_{35}b_{37}}{\omega_c^2} \\
&\quad + \frac{2b_{17}b_{35}}{2\omega_a\omega_c - \omega_c^2} - \frac{2b_{17}b_{35}}{2\omega_a\omega_c + \omega_c^2} + \frac{2b_{12}b_{36}}{\omega_a^2}, \\
\Gamma_c^2 &= -3b_{310} + \frac{10b_{37}^2}{3\omega_c^2} + \frac{2b_{19}b_{36}}{\omega_a^2} + \frac{b_{19}b_{36}}{\omega_a^2 - 4\omega_c^2}, \\
\Gamma_c^3 &= -\frac{b_{16}b_{33}}{-\omega_a^2 + \omega_c^2}, \Gamma_c^4 = \frac{2b_{18}b_{36}}{\omega_a^2}, \\
\Gamma_b^5 &= -\frac{b_{33}b_{36}}{\omega_a^2 - \omega_c^2} - \frac{b_{12}b_{33}}{3\omega_a^2}, \\
\Gamma_c^6 &= -\frac{b_{14}b_{33}}{-\omega_a^2 + \omega_b^2}, \Gamma_c^7 = \frac{2b_{15}b_{35}}{2\omega_a\omega_b - \omega_b^2} - \frac{2b_{15}b_{35}}{2\omega_a\omega_b + \omega_b^2}, \\
\Gamma_b^8 &= \frac{b_{18}b_{36}}{\omega_a^2 - 4\omega_b^2}.
\end{aligned}
$$

References

1. Guo, T.D., Kang, H.J., Wang, L.H., Zhao, Y.Y.: Cable's mode interactions under vertical support motions: boundary resonant modulation. Nonlinear Dyn. **84**, 1259–1279 (2016)
2. Su, X.Y., Kang, H.J., Chen, J.F., Guo, T.D., Sun, C.S., Zhao, Y.Y.: Experimental study on in-plane nonlinear vibrations of the cable-stayed bridge. Nonlinear Dyn. **98**, 1247–1266 (2019)
3. Guo, T.D., Rega, G.: Direct and discretized perturbations revisited: a new error source interpretation, with application to moving boundary problem. Eur. J. Mech. A Solids **81**, 103936 (2020)
4. Au, F.T.K., Cheng, Y.S., Cheung, Y.K., Zheng, D.Y.: On the determination of natural frequencies and mode shapes of cable-stayed bridges. Appl. Math. Model. **25**, 1099–1115 (2001)
5. Irvine, H.M., Caughey, T.K.: The linear theory of free vibrations of a suspended cable. Proc. R. Soc. London. A. **341**, 299–315 (1974)
6. Rega, G., Luongo, A.: Natural vibrations of suspended cables with flexible supports. Comput. Struct. **12**, 65–75 (1980)
7. Bliek, A.: Dynamic Analysis of Single Span Cables. Ph.D. Diss. Massachusetts Institute of Technology, Cambridge, MA (1984)
8. Luongo, A., Zulli, D.: Dynamic instability of inclined cables under combined wind flow and support motion. Nonlinear Dyn. **67**, 71–87 (2012)
9. Fujino, Y., Warnitchai, P., Pacheco, B.M.: An experimental and analytical study of autoparametric resonance in a 3DOF model of cable-stayed-beam. Nonlinear Dyn. **4**(2), 111–138 (1993)
10. Fung, R.F., Lu, L.Y., Huang, S.C.: Dynamic modelling and vibration analysis of a flexible cable-stayed beam structure. J. Sound Vib. **254**(4), 717–726 (2002)
11. Zhang, L.N., Li, F.C., Wang, X.Y., Cui, P.F.: Theoretical and numerical analysis of 1:1 main parametric resonance of stayed cable considering cable-beam coupling. Adv. Mater. Sci. Eng. **2017**, 1–10 (2017)
12. Lenci, S., Ruzziconi, L.: Nonlinear phenomena in the single-mode dynamics of a cable-supported beam. Int. J. Bifurcat. Chaos. **19**(3), 923–945 (2009)
13. Gattulli, V., Morandini, M., Paolone, A.: A parametric analytical model for non-linear dynamics in cable-stayed beam. Earthq. Eng. Struct. Dyn. **31**, 1281–1300 (2002)
14. Gattulli, V., Lepidi, M.: Localization and veering in the dynamics of cable-stayed bridges. Comput. Struct. **85**, 1661–1678 (2007)
15. Gattulli, V., Lepidi, M., Macdonald, J.H.G., Taylor, C.A.: One-to-two global-local interaction in a cable-stayed beam observed through analytical, finite element and experimental models. Int. J. Nonlinear Mech. **40**(4), 571–588 (2005)
16. Wei, M.H., Xiao, Y.Q., Liu, H.T.: Bifurcation and chaos of a cable-beam coupled system under simultaneous internal and external resonances. Nonlinear Dyn. **67**, 1969–1984 (2012)
17. Wei, M.H., Lin, K., Jin, L., Zou, D.J.: Nonlinear dynamics of a cable-stayed beam driven by sub-harmonic and principal parametric resonance. Int. J. Mech. Sci. **110**, 78–93 (2016)
18. Cao, D.Q., Song, M.T., Zhu, W.D., Tucker, R.W., Wang, C.T.: Modeling and analysis of the in-plane vibration of a complex cable-stayed bridge. J. Sound Vib. **331**, 5685–5714 (2012)
19. Su, X.Y., Kang, H.J., Guo, T.D.: A novel modeling method for in-plane eigenproblem estimation of the cable-stayed bridges. Appl. Math. Model. **87**, 245–268 (2020)
20. Su, X.Y., Kang, H.J., Guo, T.D., Cong, Y.Y.: Modeling and parametric analysis of in-plane free vibration of a floating cable-stayed bridge with transfer matrix method. Int. J. Struct. Stab. Dyn. **20**, 2050004 (2020)
21. Blair, K.B., Krousgrill, C.M., Farris, T.N.: Nonlinear dynamic response of shallow arches to harmonic forcing. J. Sound Vib. **194**(3), 353–367 (1992)
22. Breslavsky, I., Avramov, K.V., Mikhlin, Y., Kochurov, R.: Nonlinear modes of snap-through motions of a shallow arch. J. Sound Vib. **311**(1–2), 297–313 (2008)
23. Benedettini, F., Alaggio, R., Zulli, D.: Nonlinear coupling and instability in the forced dynamics of a non-shallow arch: theory and experiments. Nonlinear Dyn. **68**(4), 505–517 (2012)
24. Kang, H.J., Guo, T.D., Zhao, Y.Y., Fu, W.B., Wang, L.H.: Dynamic modeling and in-plane 1:1:1 internal resonance analysis of cable-stayed bridge. Eur. J. Mech. A Solids **62**, 94–109 (2017)
25. Cong, Y.Y., Kang, H.J., Guo, T.D.: Planar multimodal 1:2:2 internal resonance analysis of cable-stayed bridge. Mech. Syst. Sig. Process. **120**, 505–523 (2019)
26. Macbain, J.C., Genin, J.: Natural frequencies of a beam considering support characteristics. J. Sound Vib. **27**(2), 197–206 (1973)
27. Leissa, A.W., Qatu, M.S.: Vibrations of Continuous Systems. McGraw-Hill, New York (2011)
28. Yi, Z.P., Stanciulescu, I.: Nonlinear normal modes of a shallow arch with elastic constraints for two-to-one internal resonances. Nonlinear Dyn. **83**, 1577–1600 (2016)
29. Pi, Y.L., Bradford, M.A., Tin-Loi, F.: Nonlinear analysis and buckling of elastically supported circular shallow arches. Int. J. Solids Struct. **44**, 2401–2425 (2007)
30. Zhang, X.Y., Peng, J., Wang, L.H.: Parametric resonances in the two-to-one resonant beams on elastic foundation. Nonlinear Dyn. **77**, 339–352 (2014)
31. Ding, H., Chen, L.Q.: Nonlinear vibration of a slightly curved beam with quasi-zero-stiffness isolators. Nonlinear Dyn. **95**, 2367–2382 (2019)
32. Kloda, L., Lenci, S., Warminski, J.: Nonlinear dynamics of a planar beam–spring system: analytical and numerical approaches. Nonlinear Dyn. **94**, 1721–1738 (2018)
33. Luongo, A., Zulli, D.: Parametric, external and self-excitation of a tower under turbulent wind flow. J. Sound Vib. **330**(13), 3057–3069 (2011)
34. Belhaq, M., Kirrou, I., Mokni, L.: Periodic and quasiperiodic galloping of a wind-excited tower under external excitation. Nonlinear Dyn. **74**(3), 849–867 (2013)
35. Malhotra, N., Namachchivaya, N.S.: Chaotic dynamics of shallow arch structures under 1:2 resonance. J. Eng. Mech. **123**, 612–619 (1997)
36. Seydel, R.: Practical Bifurcation and Stability Analysis. Springer, New York (2009)

37. Nayfeh, A.H., Balachandran, B.: Applied Nonlinear Dynamics. Wiley, New York (1995)
38. Zhao, Y.B., Guo, Z.X., Huang, C.H., Chen, L.C., Li, S.C.: Analytical solutions for planar simultaneous resonances of suspended cables involving two external periodic excitations. Acta Mech. **229**, 4393–4411 (2018)
39. Nayfeh, A.H., Mook, D.T., Marshall, L.R.: Nonlinear coupling of pitch and roll modes in ship motions. J. Hydronaut. **7**(4), 145–152 (1973)